THE UNIVERSITY OF OKLAHOMA

GRADUATE COLLEGE

ANALYSIS OF THE FINITE ARRAY ON THE SCANNING PERFORMANCE OF PHASED ARRAY ANTENNAS

A THESIS

SUBMITTED TO THE GRADUATE FACULTY

in partial fulfillment of the requirements for the

Degree of

MASTER OF SCIENCE

By

KEVIN CONSTIEN
Norman, Oklahoma
2020

ANALYSIS OF THE FINITE ARRAY ON THE SCANNING PERFORMANCE OF PHASED ARRAY ANTENNAS

A THESIS APPROVED FOR THE
SCHOOL OF ELECTRICAL AND COMPUTER ENGINEERING

BY THE COMMITTEE CONSISTING OF

Dr. Jorge L. Salazar-Cerreño, Chair

Dr. Hjalti Sigmarsson

Dr. Nafati Aboserwal

Acknowledgments

I would like to begin my thanking everyone that has contributed to the work behind this thesis. First, I am thankful for Dr. Salazar for all of his guidance and support over the years. I am also grateful for my committee as a whole for their time and input. I appreciate the assistance that I have received from other members of the PAARD team. Special thanks to Dr. Aboserwal, Javier, and Jose for their feedback and contributions as well.

I would also like to express the gratitude that I have for my mother and father. Both of you have always been supportive of me no matter the situation. You have always been a source of strength for me whenever I needed it and have helped me immensely throughout my academic career. I also appreciative of the academic values that you instilled upon me during my youth which have led me to this point in my career. Without either of you this would not be possible.

Finally, I would like to thank my good friends and colleagues Tom, Armando, Gerald, Octavio, and Whitney with whom I got to share my graduate school experience with. Working alongside them has made me a better engineer, and my time with them outside of class has helped me grow as a person.

Table of Contents

List Of Figures

Abstract

Modern high performance phased array antennas require large apertures to achieve both high gain and narrow beamwidth. It is not practical to manufacture such large apertures, so the full array is composed of smaller sub-arrays known as line-replaceable units (LRU) which will then be assembled to create the final array. When the radiation patterns of an individual LRU are measured, the array will be in a finite environment. This means that the array will be impacted by edge effects, amongst other factors, which will limit the measured array scanning performance. This project focuses on the use of finite array embedded elements patterns to predict scanning performance in the full array.

First, the fundamentals of scanning array antennas are reviewed. Then, the main impacts of finite size on phased array scanning performance are discussed. In particular, theoretical phased arrays with and without both mutual coupling and diffraction fields will be used to determine the impact these factors have on antenna scanning patterns in the finite environment. The average element pattern is then introduced as a way to accurately predict scanned radiation patterns of a full array using a single element pattern. Individual antenna elements within a finite LRU are then used to reproduce theoretical scanned array patterns along the principle planes. Finally, future work is proposed to further validate the results.

Chapter 1

Introduction

1.1 Motivation

Phased array antennas offer many benefits over traditional antennas which have led them to become a popular choice for use for radar and wireless communication. These benefits include the ability to beam steer without moving parts, create multiple beams, digital beamforming, and many others. As phased arrays have become popular for use in government and industry applications, design constraints including cross-polarization levels, bandwidth, and sidelobe levels will continue to call for more complex element geometries. Unfortunately, complex element geometry becomes an issue when attempting to use EM simulators, especially when the array becomes electrically large.

Modern high performance phased array radar systems are required to have high gain and narrow beamwidth [1]. To meet these requirements, large phased arrays systems are used, composed of hundreds if not thousands of elements. When an array is very large, the array can be assumed to be infinite and floquet port analysis can be used rather than simulating the entire array. The infinite array approach allows for drastic reductions in computation time [2], but unfortunately it will not accurately represent the diffraction fields and other factors that result due to the

finite size of the array. The unit cell will assume that each element in the array is identical in terms of both physical geometry and radiation characteristics. When the array is manufactured, it will have a finite size and thus the introduction of edges to the array will add diffraction fields which will change the radiation characteristics of element depending on position and polarization.

To physically realize these electrically large arrays, the array is commonly manufactured using smaller sub-arrays known as line-replaceable units (LRU) which are then assembled to create the final array. These LRUs are smaller finite arrays with typical sizes varying from around 8x8 to 10x10 [3] meaning that the infinite array approximation will not be valid. In reality, the mutual coupling and diffraction fields in the finite array will be truncated and not necessarily be represented with a single unit cell simulation. To accurately characterize LRUs, these truncated fields need to be accounted for as they will impact mutual coupling, element radiation patterns, and the overall scanning performance of the array.

Ultimately, to accurately predict the performance of the physically realized array, the finite array must be taken into consideration. This will be done by first exploring planar array characteristics and analyzing the changes in mutual coupling, diffraction fields, and other factors that will change due to the finite size of the array. These changes in performance will then be related to show how the overall scanning performance of the array changes due to the finite size of the array.

1.2 Literature Review

The characterization of array scanning performance most often begins with the use of the unit cell in an infinite array. It is used at the beginning of the design process for many arrays as it will reveal many important characteristics of the array while also being computationally less intensive than the simulation of an electrically large array. While it is important, other methods have also been introduced to better represent the scanned element patterns and scanning range in finite array antennas.

The infinite array was first introduced by Wheeler in [4] when he conceptualized an array as a current sheet transmitting a transverse electromagnetic (TEM) mode into a waveguide. This idea was then used to provide a solution for the radiation resistance of a dipole in an infinite array. He then refined this idea in [5] where he represented the array as an infinite current sheet which is then used to derive the impedance variation with scan angle. The theory introduced by Wheeler in these papers meant that it was now possible to determine array reflections without the need to manufacture an array composed of hundreds of elements. The infinite array then became widely used in the form of the waveguide simulator which utilizes the walls to act as opposing electrical and magnetic boundary conditions.

This technique was then used by many to analyze the infinite array. It was used in [6] - [10] and others to show that the element input impedance and mutual coupling varies with scanning angle and position. In [11], Edelberg and Oliner used the waveguide model to derive the input admittance of a slot in the infinite array environment. Stark then expanded on Wheeler's work [4] by deriving the radiation impedance of an

infinite array of dipoles for an arbitrary scanning angle in [12]. Farrell and Kuhn [13] have derived a solution for an infinite array of waveguides. Array scan blindness has been studied in depth in [14] and [15].

As technology advanced, the waveguide simulator was eventually implemented in electromagnetic solvers through the use of Floquet analysis. Essentially the infinte array can be viewed as the Fourier transform of an infinite number of sources placed at regular intervals. The Fourier integral will result in a series of Dirac delta functions and the continuous Fourier spectrum will discrete spectral lines [16]. The Floquet modal series can then be expanded for the array of source functions with varying amplitudes and phases to represent the scanned beam of the array.

Scanning performance of finite arrays started to become analyzed in dipole arrays through the use of the impedance matrix in [17], [12], and [18]. These methods used measured mutual impedances along with progressive phase shifts to calculate the scan impedance for each element in the array. This was done for arrays composed of elements with simple current distributions. For finite arrays with more complex geometries, method of moment expansions could be used.

The Weiner-Hopf factorization procedure is used in [19] to analyze mutual coupling along edge elements in a semi-infinite through the use of an infinite linear array. This process allows for the calculation of the scanned reflection coefficient in the semi-infinite array in terms of an integral of phased scan impedances in the scanned reflection coefficient of the infinite array.

Ishimaru outlined a process to analyze scanning in finite periodic structures in [20] by embedding a finite array into a matrix of identical arrays. This process first

calculates the scanned element pattern for the infinite array which is then Fourier transformed back to the finite aperture. The result is then convolved with a periodic stucture of finite arrays. Finally, the result is inverse transformed over the structure to result in the scan element pattern.

A simplified version of Floquet analysis has also been done in [21] and [22] using the finite array. Using the measured mutual coupling of the finite array, the antenna can be analyzed in depth using mutual impedance, mutual admittance, and scattering parameters.

Using the previously mentioned impedance matrix method, Diamond detailed the process of calculating the scan impedance and scan element patterns for a finite array of dipoles in [18]. This was used to evaluate scanning performance of small arrays. The scan resistance and gain of the center element was shown for the principle planes and the scanned element patterns are obtained. Pozar also performed a similar analysis later in [23] where a finite array of dipoles are analyzed. Using this approach a finite dipole array was measured and mutual impedance was used to calculate the scanned element pattern. The scanned reflection coefficient was then analyzed over scan angle along with the embedded element patterns.

Scanning performance is most often evaluated to reveal any blind angles that may exist in the array. Most modern approaches to analyze scanning performance still use the impedance matrix method, but there has been work to more accurately predict blind angles. In [24], the phase of the average scan impedance was used to predict blind angles in finite dipole arrays. Scan blindness in a conformal finite phased array of printed dipoles was investigated in [25]. A hybrid method of moments/ Green's

function technique was used to incorporate mutual coupling between dipoles and surface waves. Sanadgol also uses traditional active impedance simulations of the unit cell in addition to surface wave theory to accurately represent blind angles that occur in finite arrays of printed dipoles [26].

Many methods have been used and are still used to evaluate scanning performance. The most convenient method is to use Floquet modal analysis on the unit cell of an array to obtain infinite array scanning performance. In situations where the array is finite, mutual impedances are normally measured to obtain scanned element patterns as well as the active reflection coefficient. These methods are still used to evaluate blind angles in scanning arrays, but there have been improvements in allowing for mutual coupling to be analyzed along with surface waves to accurately predict scanning performance in finite arrays.

1.3 Problem Statement

The process of designing a high performance phased array antenna typically involves the use of an electromagnetic solver to simulate the design. If the antenna is considered electrically large, then the unit cell can be used to simulate the array in the infinite array environment. While this approximation is very common, the physical array is not infinite in reality and thus this method should only be used in the case that each element can be approximated to have the same performance. The use of the infinite array approach will give an analysis of an array where each element has

the same radiation characteristics and mutual coupling effects. In reality, the manufactured array will be finite and can only be approximated with the unit cell. As such, the use of the infinite array will be compared to the finite array to determine the error that the use of the unit cell will introduce with such approximations. The primary focus of this comparison is to investigate the changes in the array scanning performance that occur with the approximations used for the infinite array.

1.4 Organization of the Thesis

The thesis is organized as follows. It begins with a review of the fundamental phased array concepts in Chapter 2. Different radiating elements are discussed along with the benefits and drawbacks that they introduce in the array environment. Basic array theory will then be covered for both linear and planar configurations. Surface waves, mutual coupling, and the active reflection coefficient will then be discussed. Chapter 3 outlines the major impacts that finite size will have on an array. This begins with an analysis of the edge effects that occur in the array. Mutual coupling will then be discussed and related to both element position and spacing. Array embedded element patterns and radiation characteristics will then be presented. The use of the active reflection coefficient will then be employed with simulated results to show how scanning performance will change with array size. These factors are then used to evaluate the overall scanning performance of the array. Chapter 4 will then analyze manufactured antennas using the techniques from Chapter 3. This will be used to compare measured scanning performance to the simulated infinite array to show the

impacts the finite array will have on the scanning performance. Finally, this thesis will conclude with Chapter 5 which presents the current state of the project and the future work that needs to be done.

Chapter 2

Fundamentals of Phased Array Antennas

2.1 Introduction

The work proposed in this thesis focuses on variations in the simulated array performance of the fully assembled array compared to the performance of smaller finite sub-arrays which will ultimately be used to create the full array. In particular, a focus will be placed on the scanning performance of arrays and the variations that occur in scanning performance due to the size of the antenna. Prior to the investigation of this topic, it would first be helpful to review some relevant concepts relating to the functionality and design of array antennas. The array will be simplified to the basic case of a uniform linear array to demonstrate the basic array theory. The factors that influence the array pattern due to physical geometry will be discussed including array geometry and spacing. This analysis will then be adjusted for the case of a planar array to investigate the pattern variation due to the introduction of grating lobes. The concept of coupling between antenna elements will then be discussed. Typical sources of scanning blindness in array antennas including mutual coupling and surface waves will then be reviewed. Finally, the active reflection coefficient will be discussed as a way to analyze scanning performance in array antennas.

2.2 Array Characteristics

The phased array antenna is generally composed of some arbitrary number of radiating elements which each have their own amplitude and phase. The antenna radiation pattern can then be represented as the spacial Fourier transform of each element excitation. The array pattern can also be viewed more intuitively as the product of the isolated element pattern and the array factor. This concept will be explored further below in the context of a linear array.

2.2.1 Linear Array Characteristics

The radiation pattern of the array is related to the radiation patterns of each individual element along with the element positions and excitations. For simplicity, a uniform linear array will be used to illustrate this concept. The array will be composed of N elements aligned along the x-axis ($\phi = 0$) for scanning in the $\hat{\theta}$ direction. If each element has an identical radiation pattern, then the array pattern can be expressed by

$$\boldsymbol{F(\theta)} = \boldsymbol{f_i}(\theta) \sum_{n=1}^{N} e^{j(n-1)\psi} \tag{2.1}$$

where $\psi = kd\sin\theta + \beta$, $\boldsymbol{f_i}$ is the isolated element pattern of the array, k is the propagation constant $2\pi/\lambda$, d is the element spacing, and β is the progressive phase shift. It can be seen that the array pattern is simply the product of the isolated element pattern and a phase term which is better known as the array factor.

The array factor of the uniform array can be altered physically through the element spacing or by adding a progressive phase shift between elements using T/R modules or various other phase shifting techniques. This phase shift between array elements can be used to steer the main beam of the array to a desired angle of θ. It can be calculated for the uniform linear array by the expression

$$\beta = -kd\sin\theta_0 \tag{2.2}$$

where θ_0 is the desired scan angle. This can easily visualised using simple geometry seen in figure 2.1. The elements are uniformly separated by some distance d, so the distance to the desired scanning angle is $d\sin\theta$ which is simply multiplied by the propagation constant to find the necessary phase shift.

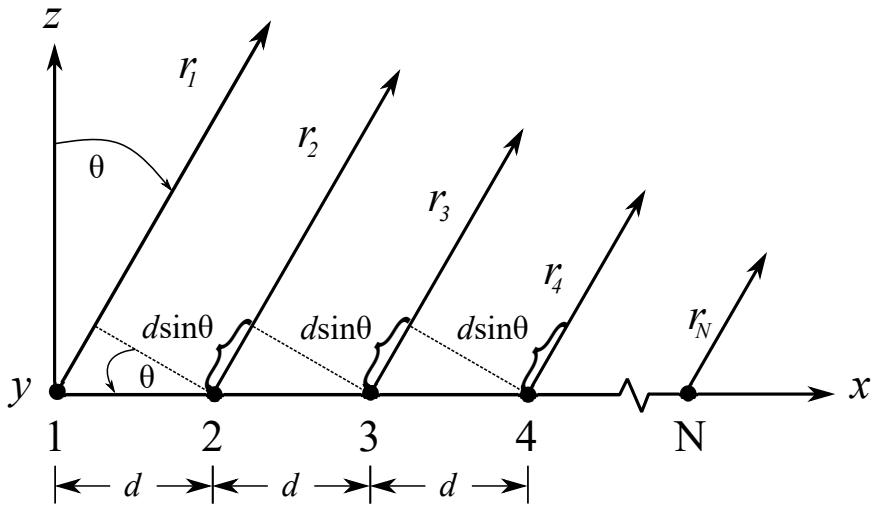

Figure 2.1: Progressive phase shift between array elements in a linear array.

This simple change in array factor is what sets phased arrays apart from traditional antennas allowing for the ability to scan the main beam of the array without any moving parts. It is becoming more common to physically realize these phase shifting

techniques through the use of fully digital phased arrays which use T/R modules on each element, but other feeding techniques can be used to create progressive phase shifts. In particular, the use of a series-fed phased array allows for the array to be fed using only a single source and then a progressive phase shift can be accomplished by adjusting the frequency of the source thus adjusting the propagation constant.

As mentioned above, the array factor is a function of the spacing between elements and their respective excitations. The element spacing will dictate the visible region of the array. The visible region can be viewed as the extent of the array factor which is visible in the array pattern. It can be represented by

$$VR = 2kd \tag{2.3}$$

where d is the inter-element spacing and k is the propagation constant. The spacing of the typical array is chosen to be half-lambda so that the visible region will be 2π and there will only one main beam when scanning the array in the $\hat{\boldsymbol{\theta}}$-direction to $\pm 90^{\circ}$. If the visible region is larger than π, then there will be another maximum in the array factor leading to the creating of a grating lobe.

The grating lobe is the primary reason that half-lambda spacing is chosen. When the spacing is increased the main beam of the array may be split depending on the scanning angle and the spacing thus leading to a decrease in main beam power and an increase in grating lobe radiation. In short, grating lobes are not desired so arrays are

designed so that they do not occur. The grating lobe location can be easily calculated using

$$\frac{d}{\lambda} = \frac{1}{\sin\theta_0 + \sin\theta_{GL}} \tag{2.4}$$

where θ_0 is the maximum scan angle and θ_{GL} is the angle that the grating lobe will occur. For half-lambda spacing, the first grating lobe will occur at $\theta = +90$ degrees when the array is scanned to 90 degrees.

2.2.2 Planar Array Characteristics

The analysis of the planar array is the same as a linear array, but with the addition of another dimension. Previously the $\hat{\boldsymbol{\phi}}$ direction was held constant at 0, but it can be scanned in the planar array so it is useful to use the spherical coordinate system. The direction cosine space will be used to for this purpose allowing for the use of $\hat{\boldsymbol{u}}$ and $\hat{\boldsymbol{v}}$.

$$\hat{\boldsymbol{u}} = \sin\theta\cos\phi \tag{2.5}$$

$$\hat{\boldsymbol{v}} = \sin\theta\sin\phi \tag{2.6}$$

As mentioned above, the array pattern of an array is simply the spacial Fourier transform of each element excitation and position. The pattern of the planar array can still be represented using equation 2.1, but with the addition of another dimension. Again, this analysis will follow the assumption that each element in the array has

the same radiation pattern. Ignoring mutual coupling, the array pattern of a planar array is given by [27] to be

$$\boldsymbol{F(u,v)} = \boldsymbol{f_i(u,v)} \sum_{n=1}^{N} \sum_{m=1}^{M} e^{jk[(n-1)d_x(u-u_0)+(m-1)d_y(v-v_0)]} \tag{2.7}$$

where $\boldsymbol{f_i(u,v)}$ is the isolated element pattern, d_x and d_y are the inter-element spacings in the $\hat{\boldsymbol{x}}$- and $\hat{\boldsymbol{y}}$-directions respectively, and u_0 and v_0 are the steering directions in the $\hat{\boldsymbol{u}}$ and $\hat{\boldsymbol{v}}$ planes, respectively.

The array factor is now dependent of phase terms in both the $\hat{\boldsymbol{u}}$ and $\hat{\boldsymbol{v}}$ allowing for the theoretical ability to scan the beam over the hemisphere of the phase of the array. Progressive phase shifts between elements in both the $\hat{\boldsymbol{x}}$- and $\hat{\boldsymbol{y}}$-directions allow for this possibility.

The concept of the visible region of the array mentioned above comes in useful with the planar array. The grating lobes will occur based on both inter-element spacings and the direction of the main beam angle along the $\hat{\boldsymbol{\theta}}$- and $\hat{\boldsymbol{\phi}}$-axes. The visible region of the array can be viewed in sine space as a function of the main beam angle. A grid array is created in figure 2.2 using

$$u_p = u_0 + \frac{p\lambda}{d_x}, \quad p = 0, \pm 1, \pm 2, ... \tag{2.8}$$

$$v_q = v_0 + \frac{q\lambda}{d_y}, \quad q = 0, \pm 2, \pm 2, ... \tag{2.9}$$

and plotted along the inverse element spacing lattice to show the angles that grating lobes occur. The inner circle in figure 2.2 represents the visible region of the array.

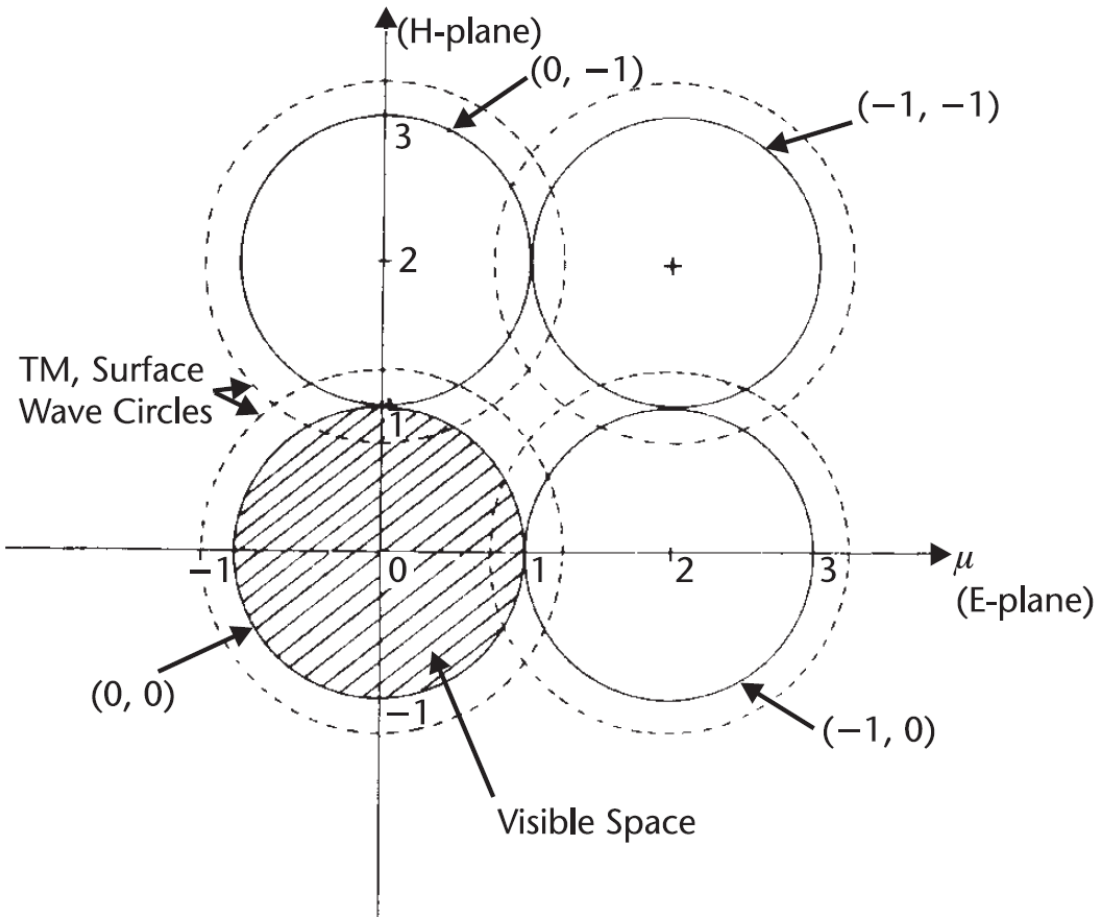

Figure 2.2: Grating lobe diagram for a planar array, adapted from [27].

The intersections between the visible region and the surrounding circles represent the scan angles where a grating lobe will occur.

2.3 Radiating Elements for Phased Arrays

Phased array antennas have been created using many different radiating elements, but most fall under the category of either a wire antenna, aperture antenna, or patch antenna. In this section, radiating elements falling into each of these categories will be discussed briefly along with the benefits and drawbacks that occur when using them.

Wire antennas are created out of various shapes of wire to form a radiator. Common shapes include a loop, helix, and simply a straight wire. The half-wave dipole is simply a straight wire and perhaps the most well studied radiating structure. It is therefore very well defined using closed-form equations [28]. The half-wave dipole is composed of two center-fed arms of length $\lambda/4$ each to result in an overall size of $\lambda/2$. The electric and magnetic field components of the dipole will be given by

$$E_\theta \simeq j\eta \frac{I_0 e^{-jkr}}{2\pi r} \left[\frac{\cos(\frac{\pi}{2}\cos\theta)}{\sin\theta} \right] \tag{2.10}$$

$$H_\phi \simeq j \frac{I_0 e^{-jkr}}{2\pi r} \left[\frac{\cos(\frac{\pi}{2}\cos\theta)}{\sin\theta} \right] \tag{2.11}$$

Total radiated power, directivity, and radiation resistance can then be calculated from equations 2.10 and 2.11. The simple geometry means that it can be well defined through closed-form solutions because they have known current distributions. It has been widely studied and used in scanning arrays in the form of the printed dipole array. The printed dipole still remains an excellent candidate for use in scanning arrays due to its simplicity geometry and compatibility with modern fabrication techniques. It can also be designed for moderate bandwidths through the use of an integrated balun. Despite the many positives of using printed dipoles, this antenna only has a single polarization, so the printed dipole cannot be used for polarimetric radars.

An aperture antenna is created using a cutout in the surface of a conductor to create an aperture for a guided wave to radiate from. Common forms of aperture

antennas include slot antennas, horn antennas, and waveguides. The current distribution for these elements isn't as simple as in a wire antenna, but a complementary antenna can be found as in figure 2.3 and Babinet's Principle can be used to relate the slot to a dipole. Slot antenna arrays can be easily manufactured by cutting slots in the side of a waveguide. This will allow for better power handing than using a dipole array, but the array will need to be series fed meaning beam steering will need to be achieved using frequency-scanning. Like dipoles, slot antennas also only have a single polarization which make it impractical for use in polarimetric radars.

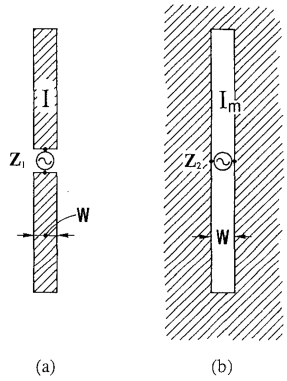

Figure 2.3: Self complementary antennas: (a) A planar dipole antenna. (b) A complementary slot antenna, adapted from [29].

The microstrip patch antenna is perhaps the most well used element type for array applications. The patch antenna is low-profile, inexpensive, and can be easily manufactured using modern microstrip techniques. Patch antennas can be easily integrated into the printed circuit board along with the rest of the circuit allowing for the addition of monolithic microwave integrated circuits (MMIC) for use as amplifiers and phase shifters.

Many patch shapes can be used, but they are most often either rectangular or circular geometries are chosen. Various methods have be used to model these geometries

including transmission-line, cavity, and full-wave models. While the transmission-line model is not as accurate as the cavity model and full-wave simulations, it allows for a more intuitive understanding of how a patch works. For a rectangular patch, the transmission-line model will represent the two radiating edges of the patch as two parallel slots with an equivalent admittance given by the substrate height, dielectric constant, and patch width. The equivalent circuit model is shown in figure 2.4.

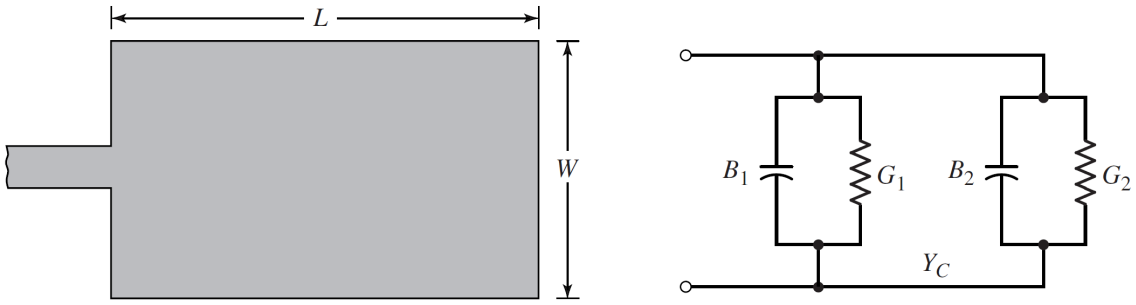

(a) Rectangular patch (b) Transmission model equivalent

Figure 2.4: A rectangular patch and the equivalent transmission-line model, adapted from [28].

A number of equations were formulated in [30] to accurately design the patch. First an effective dielectric constant for the patch is formulated. When the width of the patch is larger than the thickness of the substrate, the effective dielectric constant is given by [28]

$$\epsilon_e = \frac{\epsilon_r + 1}{2} + \frac{\epsilon_r - 1}{2}\left[1 + 12\frac{h}{W}\right]^{-1/2} \tag{2.12}$$

where W is the width of the patch, h is the substrate height, and ϵ_r is the relative permittivity of the substrate. The effective permittivity is then used to calculate the extension because of the fringing fields on the edges of the patch using [28]

$$\frac{\Delta L}{h} = 0.412 \frac{(\epsilon_e + 0.3)\left(\frac{W}{h} + 0.264\right)}{(\epsilon_e - 0.258)\left(\frac{W}{h} + 0.8\right)} \tag{2.13}$$

where ΔL is the additional length gained by the patch due to fringing fields. Finally, the resonant frequency of the patch is calculated for the dominant TM_{010} mode [28].

$$(f_{rc})_{010} = \frac{1}{2(L + 2\Delta L)\sqrt{\epsilon_e}\sqrt{\mu_0 \epsilon_0}} \tag{2.14}$$

2.4 Mutual Coupling

Typical array analysis, including previous analysis in this chapter, makes a few assumptions about the array characteristics to create simple equations to describe radiation characteristics. The current distribution of each radiating element is assumed to be known, proportional to element excitation, constant with scan angle, and all radiators are assumed to be identical. For a physically realizable antenna, none of these assumptions hold true. In reality, the current distribution of each element will vary with position, element geometry, and element excitation amongst other factors. Element radiation patterns are dependent on these factors primarily because of interactions between elements commonly referred to as mutual coupling.

When an antenna is surrounded by one or more antennas, part of the radiated energy from one antenna will be coupled to the other. The amount of coupled energy

will vary depending on the element radiation characteristics, inter-element separation, and antenna polarization. The inevitable presence of mutual coupling in the array environment means that the isolated element radiation characteristics will differ from the performance seen in the array environment. Each element will experience some amount of mutual impedance due to interactions between elements which will impact each radiator in the array differently depending on the element location in the finite array.

Coupling can happen in the feed network of the array but, can be minimized through proper impedance matching. This allows for the array to be modeled as an array of independent generators with their own source voltages and impedances. With this approach each element will have a voltage given by

$$\begin{aligned} V_1 &= Z_{11}I_1 + Z_{12}I_2 + \cdots + Z_{1N}I_N \\ V_2 &= Z_{12}I_1 + Z_{22}I_2 + \cdots + Z_{2N}I_N \\ &\vdots \\ V_N &= Z_{1N}I_1 + Z_{2N}I_2 + \cdots + Z_{NN}I_N \end{aligned} \tag{2.15}$$

where V_n and I_n are the voltage and current in the n^{th} element. The mutual impedance Z_{mn} will then be given by

$$Z_{mn} = \left.\frac{V_m}{I_n}\right|_{I_{i=0}}, \forall i \neq n \tag{2.16}$$

when all other elements are open-circuited.

In practice mutual coupling is difficult to compute, but studies have been done to characterize mutual impedance. In general the following trends have been observed

for mutual coupling in arrays [31]. Coupling will be related to the embedded element pattern of the element in the array and more coupling will be seen in elements with broader radiation patterns. Elements with polarizations that are aligned parallel will experience more coupling when aligned collinear. Finally, the magnitude of mutual impedance will decrease as distance between radiators increases. This effect is illustrated in figure 2.5 which shows the mutual impedance seen by a dipole when another element is place parallel at varying distances.

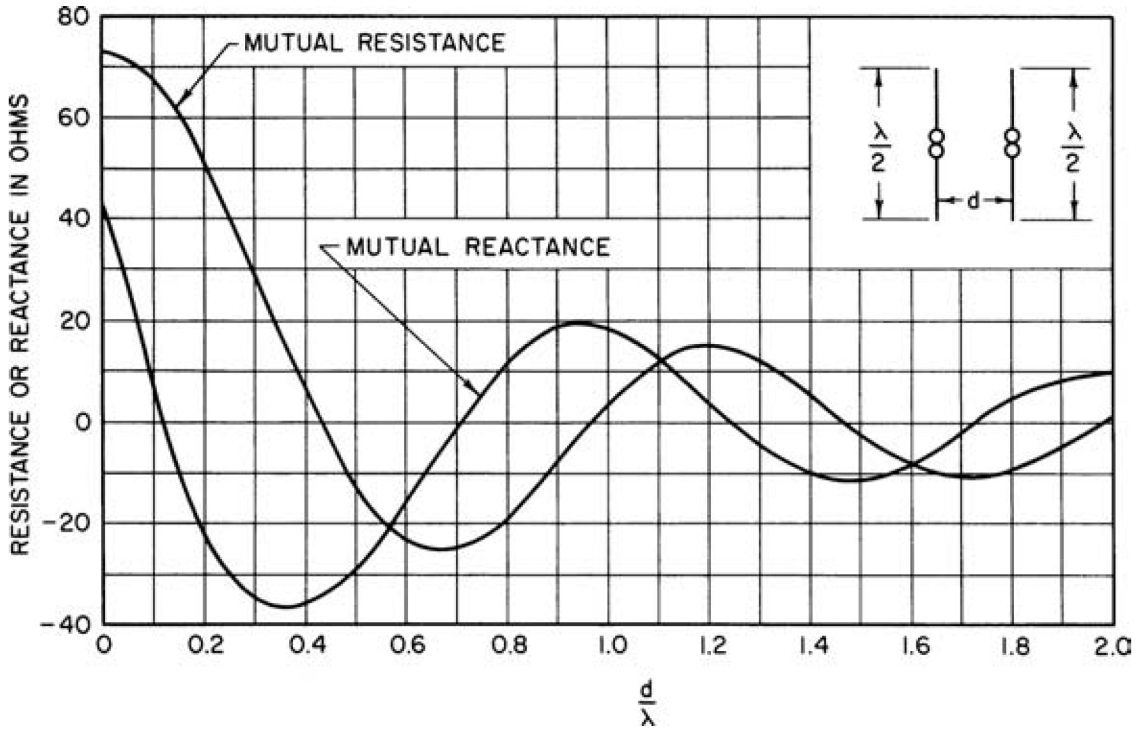

Figure 2.5: Mutual impedance between dipoles of varying distance, adapted from [32].

2.5 Active Reflection Coefficient

As previously stated, the array scan impedance will depend on the steering angle of the array. This scan dependence can easily be shown mathematically by viewing the

array as an infinite current sheet carrying charge parallel to an axis as proposed by Wheeler [5]. Figure 2.6 shows the case of the current sheet in receiving mode in the the $E-$ and $H-$plane.

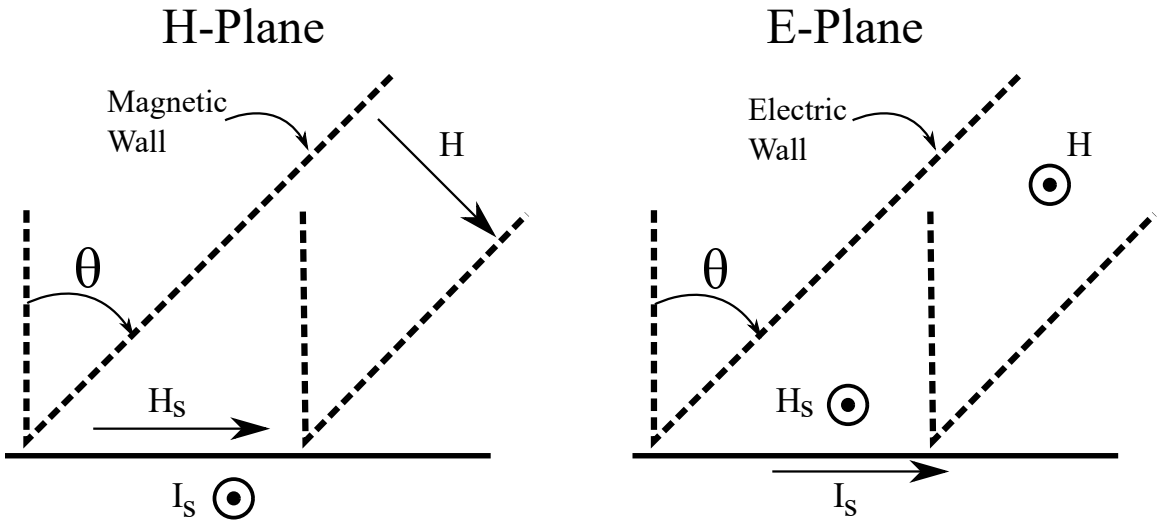

Figure 2.6: Current sheet plane of scan, adapted from [5].

If the array is matched to the impedance of free space at normal incidence when $\theta = 0$, then there will be an impedance mismatch over scan angles. In the $H-$plane, an oblique incident wave will see a section of the current sheet that is larger than the wavefront, thus the apparent resistance is decreased by $\cos\theta$. The reflection coefficient will be

$$\Gamma = \frac{\cos\theta - 1}{\cos\theta + 1} = -\tan^2\frac{\theta}{2} \tag{2.17}$$

Oblique incidence in the $E-$place will give the opposite result. The seen section of the current sheet seen will be smaller than the wavefront and the resistance will increase giving the reflection coefficient

$$\Gamma = \frac{1 - \cos\theta}{1 + \cos\theta} = \tan^2\frac{\theta}{2} \tag{2.18}$$

The above cases are for the case of an array in receiving mode. Typically the antenna reflection coefficients are viewed from the perspective of the array transmitting, so the coefficient sign will be reversed in this case.

Physical antennas will obviously perform differently than viewing the array an infinite current sheet, but this experiment establishes that the impedance seen by the antenna element will change with respect to the scan angle. This is known as the scan or active impedance which be shown to be a useful tool in analyzing array scan performance. The array can then be analyzed in the case where the array is driven by free or forced excitation.

In the case of forced excitation, each element will be driven with some constant voltage and the phase will be altered for beam-steering. The element currents will then be a function of the driven voltage and the impedance matrix

$$[V] = [Z][I] \tag{2.19}$$

where the impedance matrix contains all inter-element impedances and is given by

$$Z = \begin{bmatrix} Z_{11} & Z_{12} & \cdots & Z_{1N} \\ Z_{21} & Z_{22} & \cdots & Z_{2N} \\ \vdots & \vdots & \ddots & \vdots \\ Z_{N1} & Z_{N2} & \cdots & Z_{NN} \end{bmatrix} \tag{2.20}$$

where the mutual impedances will be measured between each element with respect to another while the rest of the array is open circuited. The full array pattern can

then be viewed as the sum of element patterns with coefficients given by current on each radiator multiplied by the isolated element pattern. The array scan impedance will be given by [33]

$$Z_a = \sum_p \sum_q Z_{nm,pq} \frac{I_{pq}}{I_{nm}} \tag{2.21}$$

where $Z_{nm,pq}$ is the mutual impedance between the "nm" and "pq" elements.

This type of approach assumes that each element is fed by a constant voltage source. In practice, impedance mismatches between the radiators and feed network will decrease the applied voltage. It is more practical to use the free excitation viewpoint where the feed network can be viewed as a voltage source in series with some resistance leading to a constant available power source. Constant power sources can then be viewed using scattering parameters.

$$[V_r] = [S][V_i] \tag{2.22}$$

where V_i and V_r are the incident and reflected voltages. Equation 2.21 can be rewritten in terms of the scattering parameters to find the active reflection coefficient Γ_a for element nm using

$$\Gamma_a = \sum_p \sum_q S_{nm,pq} \frac{A_{pq}}{A_{nm}} \tag{2.23}$$

where the element excitation coefficient A will vary in phase between elements when scanning and in amplitude if a taper is used to decrease sidelobes.

As mentioned earlier, impedance will change with scan angle so it intuitively makes more sense to view the spacial active reflection coefficient

$$\Gamma_a = \sum \sum S_{nm} e^{-jk(nu+mv)} \tag{2.24}$$

so that reflections can be seen for any scan angle of the array. All that is needed for this calculation is the element positions and the scattering matrix. Unfortunately, it is difficult to theoretically calculate the coupling coefficients, but a network analyzer can easily be used to measured them in a physical array. The active reflection coefficient proves very useful when determining angles of blindness that will occur when scanning an array.

2.6 Scan Blindness

In some arrays, there will be some steering angles at which little to no power will be radiated, also known as blind angles. This phenomenon can be caused by mutual coupling or surface waves and is commonly analyzed using either the active reflection coefficient or scan impedance. At certain beam angles, the reflection coefficient can be increased to near unity resulting in cancellation of the main beam. Likewise, the array radiation pattern will experience a null at the same angle. Blindness typically occurs when a higher order mode cancels the dominant mode. These higher order modes can either be produced internally or externally to the antenna. Blindness in phased arrays is often said to be caused by "surface waves". This terminology is often misleading and has essentially become a way to describe blind angles regardless of the

source of blindness. There are many types of blindness that can occur, but a couple common ones will be discussed here.

The antenna substrate is a dielectric slab which will support TE and TM modes which can impact the antenna radiation depending the dielectric constant and substrate height. The propagation constant of these supported modes can be solved for as given by the procedure in [34] using transcendental equations. For a grounded dielectric slab of thickness d and permittivity ϵ_r propagation will be assumed in the $+z$-direction. There will be two regions, inside the dielectric and the free-space above the dielectric. For a TM mode the cutoff wave numbers for each region will be defined as

$$k_c^2 = \epsilon_r k_0^2 - \beta^2 \tag{2.25}$$

$$h^2 = \beta^2 - k_0^2 \tag{2.26}$$

and general solutions to the wave equations in each region can be found. boundary conditions can then be applied and a non-trivial solution can be obtained. After some simplification that following transcendental equations will result

$$(k_c d)^2 + (hd)^2 = (\epsilon_r - 1)(k_0 d)^2 \tag{2.27}$$

$$k_c d \tan k_c d = \epsilon_r h d \tag{2.28}$$

and the cut-off frequency of the TM modes will be given by:

$$f_c = \frac{nc}{2d\sqrt{\epsilon_r - 1}}, \quad \text{for} \quad n = 0, 1, 2, \cdots \tag{2.29}$$

Using numerical methods, the transcendental equations are solved to determine the supported TM modes. Figure 2.7 shows the plotted solutions for the cutoff frequencies of supported TM modes in the array substrate. This process can easily be repeated to solve for the supported TE modes. The resulting transcendental equations will be:

$$k_c^2 + h^2 = (\epsilon_r - 1)k_0^2 \tag{2.30}$$

$$-k_c d \cot k_c d = hd \tag{2.31}$$

with a TE cutoff frequency given by

$$f_c = \frac{(2n-1)c}{4d\sqrt{\epsilon_r - 1}} \quad \text{for} \quad n = 1, 2, 3, \cdots \tag{2.32}$$

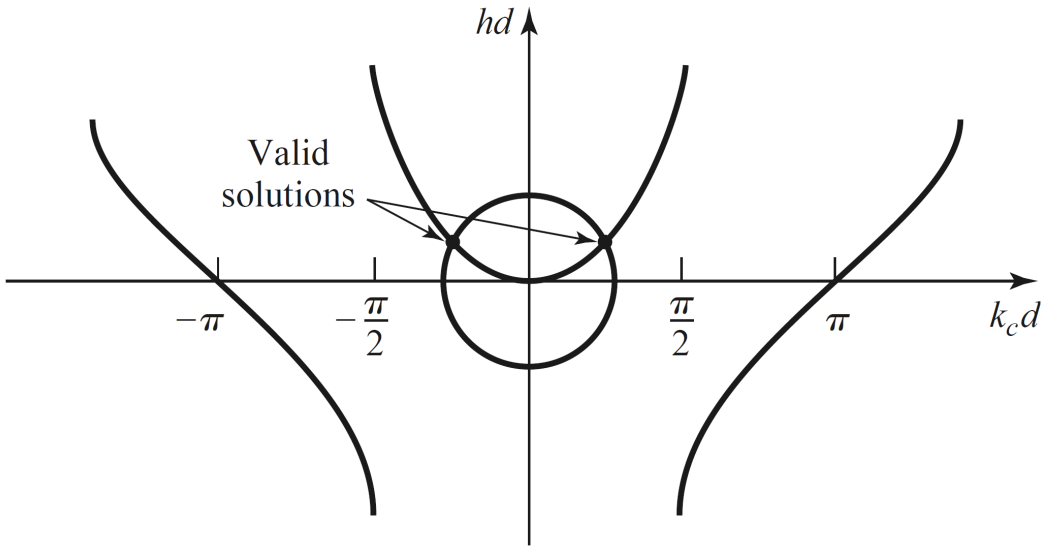

Figure 2.7: Graphical solution of the transcendental equation for the cutoff frequency of the TM surface wave mode, adapted from [34].

2.7 Summary

This chapter focused on the fundamental array theory that will be referenced throughout this thesis. It began by reviewing the concept of scanned array antennas and the use of applying a progressive phase shift along the array to accomplish beam-steering in a linear array. Planar array scanning was then discussed along with both the visible region and the concept of grating lobes. Radiation characteristics of both dipoles and rectangular patches were then reviewed. Mutual coupling in the form of inter-element mutual impedance was then discussed and with the active or scanned reflection coefficient. Finally, the topic of scan blindness was reviewed by calculating the additional supported TE and TM modes that an antenna substrate will support. These fundamental concepts will be used again in Chapter 3 when the finite array is

explored more in depth and in chapter 4 when a method to predict full array patterns is proposed.

Chapter 3

Finite Phased Array Analysis

3.1 Introduction

Modern phased array radars for weather applications require an antenna with a high gain, a narrow beamwidth, and high spacial resolution. To meet these requirements, the array needs to have an electrically large aperture which could have a size of around 8 meters by 8 meters in some cases. When the array is very large, the infinite array approach can be used to get a prediction of array performance, but it is not entirely accurate. To physically realize the array, the aperture must be divided into smaller subarrays which can then be assembled to create the full array. Sizes of subarrays may vary, but may be around 8 elements by 8 elements and therefore can't be considered as infinite. To accurately reflect the performance of the full array, the finite size of these subarrays must be considered.

An infinite array will be composed of elements with identical performance in terms of radiation patterns, reflection coefficients, mutual coupling, and scanning performance. To accurately model a large array, these assumptions cannot be made for the subarrays that are used to create the full radar system. Most notably, both the co-polar and cross-polar radiation patterns of array elements will change due to diffraction fields that are introduced by the edges of the array. Mutual coupling in

the array will also change in the array depending on element position and number of neighboring elements. This chapter will address these changes and others that occur due to the finite size of the array and analyze how the size will alter array scanning performance.

3.2 Radiating Element

A dual-polarized microstrip patch antenna with differential feeding was chosen as the radiating element for the simulated data seen throughout this chapter and in Chapter 4. Differential feeding was chosen to both decrease cross-pol levels and allow for even excitation of the element for symmetric radiation. To decrease computation time, feeding was accomplished in simulation using two coaxial probes rather than a complex feed network. Two probes fed 180 degrees out of phase were used for each polarization. Figure 3.1a shows how the radiating element is fed. The element is designed for a center frequency of 3 GHz and $\lambda/2$ spacing was chosen to eliminate grating lobes. Antenna design is not the focus of this project, so the element was designed to be geometrically simple to decrease computation times.

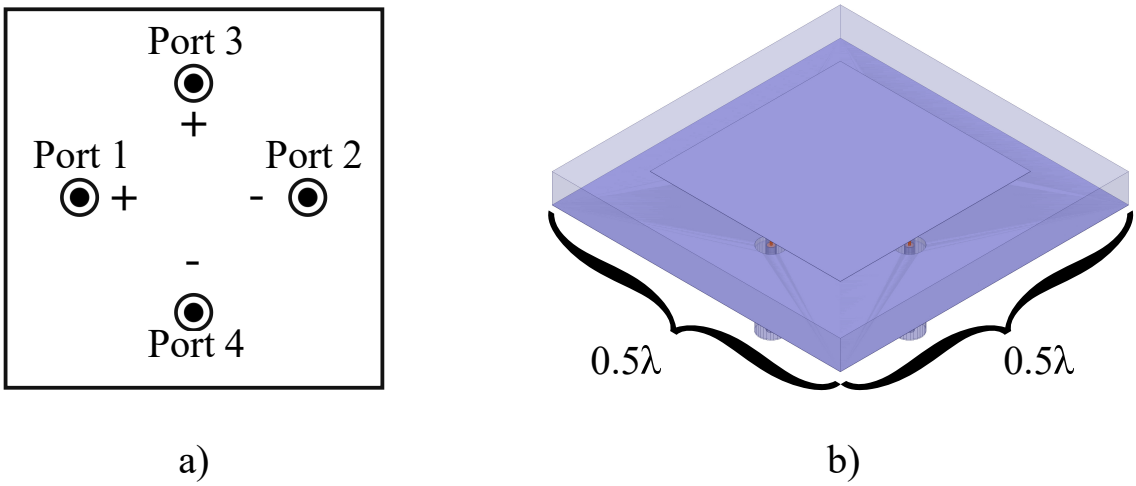

Figure 3.1: (a) A cartoon showing the radiating element port layout. (b) The radiating element unit cell in HFSS.

3.3 Diffraction Fields

The reality of the finite array is that no matter how large it may be, a planar array will always have edges. These edges will diffract the fields radiated by the antenna resulting in diffraction fields that are commonly referred to as "edge effects". The impact of edge effects will change depending on element position and polarization and as a result each element in the array will have a unique radiation pattern. The main factors attributing to edge effects in phased arrays will be discussed including ground plane size, element position, and polarization. In this section, it is desired to look only at the impacts that are caused due to edge effects and as such mutual coupling will be mitigated by using only simulations of isolated elements. Mutual coupling will be explored in more detail in Section 3.4.

The finite size of the array ground plane will introduce ripples in the radiated patterns. The size of the ground plane will change the number of ripples introduced

in the pattern and the position of the element in the ground plane will determine how symmetric the pattern is. If an element is placed at the center of the ground plane, the number of ripples in the radiation pattern will increase symmetrically as the size of the ground plane increases as shown in figure 3.2. While ripples are introduced in the co-pol patterns, only minor changes will be seen in the cross-polarization patterns of the antenna due to symmetric ground plane.

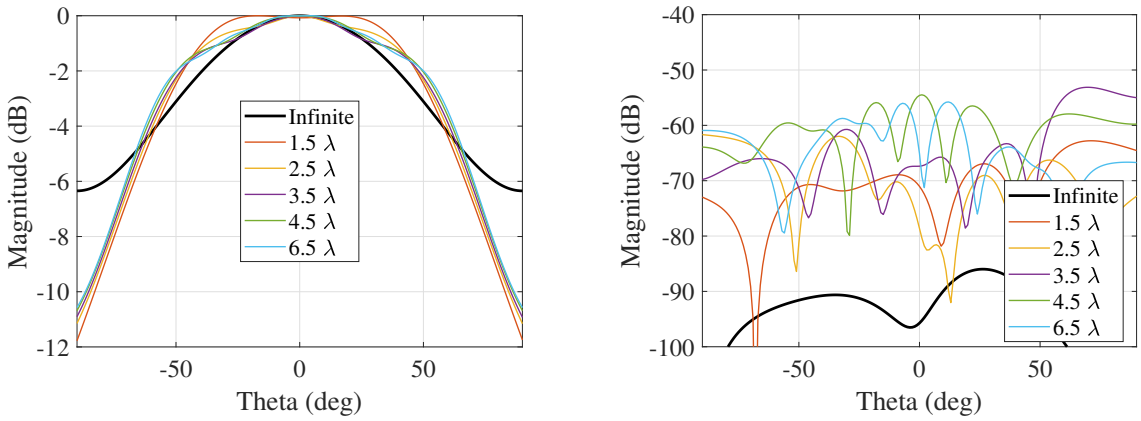

(a) (b)

Figure 3.2: E-plane radiation patterns of an isolated microstrip patch antenna on a ground plane of finite size. (a) co-pol radiation, (b) cross-pol radiation.

Edge effects will have the most notable impact when an element is not located at the center of the ground plane because the diffraction fields are no longer symmetric. This will alter both the co- and cross-pol radiation patterns in different ways. For example, when a dual polarized element is polarized in the $\hat{\mathbf{x}}$-direction and offset by 0.125λ from the center of a 4λ by 4λ ground plane in the $+\hat{\mathbf{x}}$-direction, the ripples introduced due to diffraction fields will mean the radiation pattern is no longer symmetric. There is little to no change in the radiation patterns with respect to an offset in the $+\hat{\mathbf{y}}$-direction because the element is polarized in the opposite direction.

However, if this offset is applied and the element is polarized in the $\hat{\mathbf{y}}$-direction then the same effect would be seen.

A similar impact will be seen in the cross-pol of the isolated element. If the same 0.125λ offset is applied in the $+\hat{\mathbf{x}}$-direction, no change will be seen in cross-polarization levels for an element polarized in the $\hat{\mathbf{x}}$-direction despite changes in co-pol radiation because the cross-pol fields are still symmetric. However, if the same 0.125λ offset is applied in the $+\hat{\mathbf{y}}$-direction, cross-pol diffraction fields will no longer be symmetric and an increase in cross-pol levels will be seen.

These simulations have been performed for a dual-polarized isolated microstrip patch antenna polarized in the $\hat{\mathbf{x}}$-direction and placed on a finite ground plane of size 4λ by 4λ. The patch was then offset by 0.125λ in the $+\hat{\mathbf{x}}$-direction. This offset was then applied in the $+\hat{\mathbf{y}}$-direction, and then in both directions. E-plane co- and cross-pol patterns are seen in figure 3.3. It is shown that element radiation patterns will be negatively impacted along a plane in which asymmetric diffraction fields will occur. For this simulation, co-pol diffraction fields are asymmetric in the E-plane when the element is offset in the $+\hat{\mathbf{x}}$-direction and cross-pol diffraction fields in the E-plane are asymmetric when the element is offset in the $+\hat{\mathbf{y}}$-direction.

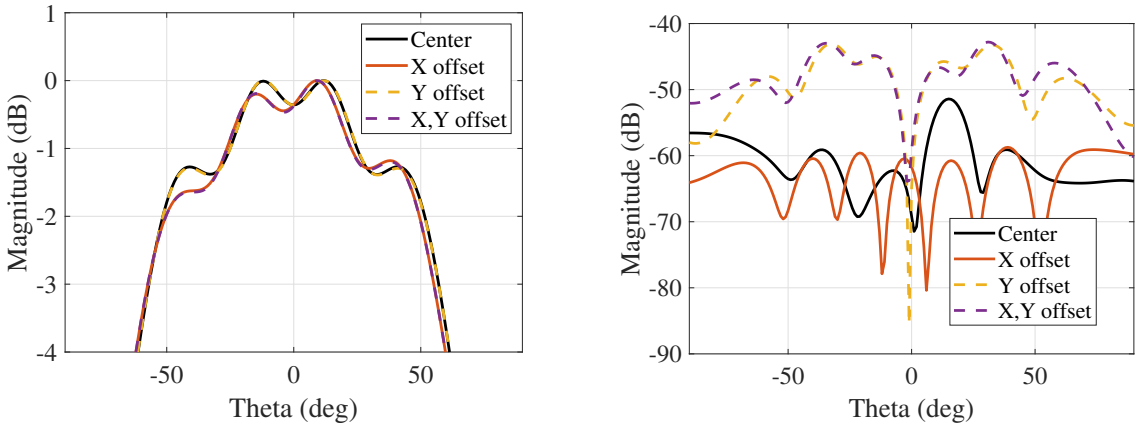

(a) (b)

Figure 3.3: E-plane normalized radiation patterns of a horizontally polarized isolated element offset 0.125λ from the center of the array. (a) co-pol radiation, (b) cross-pol radiation.

Finite array size will mean that diffraction fields will never be symmetric unless the element is located in very center of the array. Practically speaking, in a sub-array of 8 by 8 elements, the four central elements will have very similar radiation patterns. However, each element in the array will experience different uneven diffraction fields based on the position of the array. This will especially be seen in elements that are located on the edges of the array as shown in figure 3.4. For example, when a patch is polarized in the $\hat{\mathbf{y}}$-direction and then moved to a corner of the array, there will no longer be symmetry in the diffraction fields in both the co- and cross-pol directions. Therefore, co-pol radiation pattern will be uneven and the cross-pol levels will be increased in the principle planes compared to an element in the center of the array. Likewise, if the same element is positioned near the center of the $+\hat{\mathbf{y}}$ edge then co-pol diffraction symmetry will be maintained and a symmetric pattern will be seen.

However, for cross-polarization symmetry is not maintained with this positioning resulting in higher cross-pol levels.

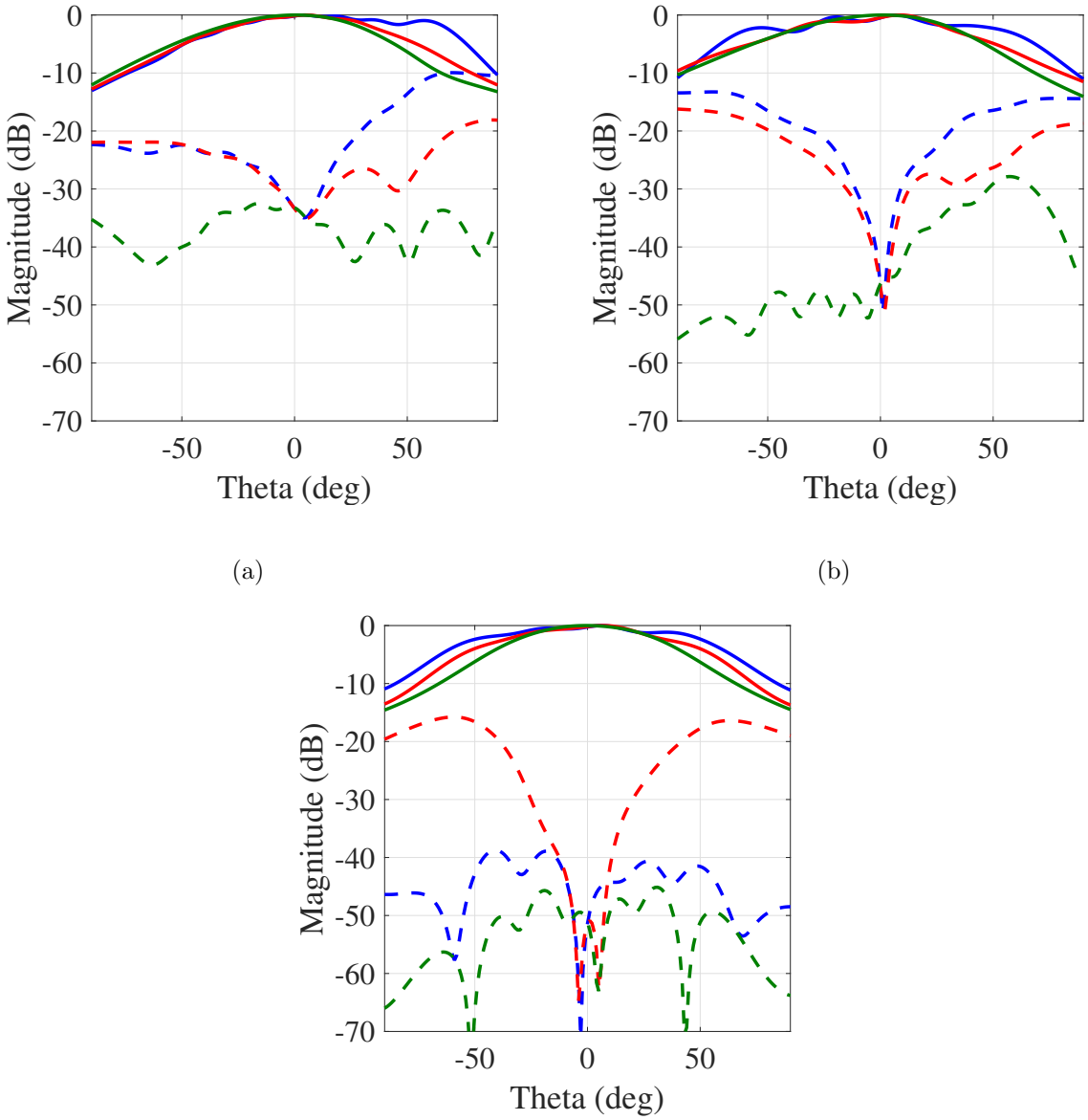

(a)

(b)

(c)

Figure 3.4: E-plane (blue), D-plane (red), and H-plane (green) co-polar (solid) and cross-polar (dashed) radiation patterns of an isolated element on a ground plane of finite size located at (a) corner (b) edge (c) center.

3.4 Mutual Coupling

The total gain of the array will be related to the gain of each individual element in the array. While each element may share the same geometry, gain will vary from the isolated element because of electromagnetic coupling between elements known as mutual coupling. Inter-element coupling will change depending on the size of the array, element spacing, position, and geometry. There have been attempts to characterize this coupling, but unfortunately this is not an easy task as each element will have unique radiation characteristics especially when the array is finite. In this section, mutual coupling will be analyzed in the finite array to show its impact on scanning performance.

Intuitively, when an array is larger, there are more elements to couple to and therefore higher levels of inter-element coupling will be seen throughout the array. While more elements will be present in the array, coupling levels drastically decrease with distance no matter the size of the array. Four different dual-polarized phased arrays were simulated with the same geometry with varying sizes to compare mutual coupling levels. The E- and H-plane coupling values to the center element are seen in figure 3.5. It is seen especially that coupling in the H-plane decreases rather predictably with position no matter the size of the array. In the E-plane, results are similar, but not as symmetric based on location. This is because the patch is fed using a single coaxial probe and is therefore unbalanced in the E-plane.

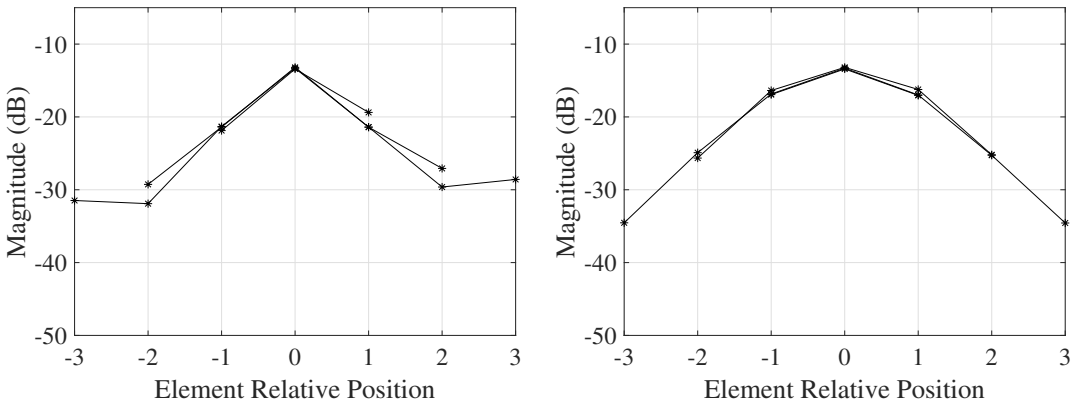

(a) (b)

Figure 3.5: Coupling to center element in a linear array. (a) E-plane (b) H-plane.

3.4.1 Element Spacing

Traditionally $\lambda/2$ spacing between elements is used in phased array design, but adjusting this distance will have a clear effect on mutual coupling. A finite 7x7 patch array will be used to demonstrate this case. Inter-element spacing is adjusted at intervals from 0.4λ to 0.7λ and an infinite ground plane is used to mitigate the diffraction fields that will occur so that only mutual coupling can be analyzed. The 2D graph of the scattering matrix of the center element shows the expected results in figure 3.6. When the elements are closer, higher levels of coupling are seen. This is much more dramatic when the embedded element pattern of the same element is shown. As element spacing is decreased, the embedded element pattern begins to broaden. Likewise, larger spacings result in narrow radiation patterns.

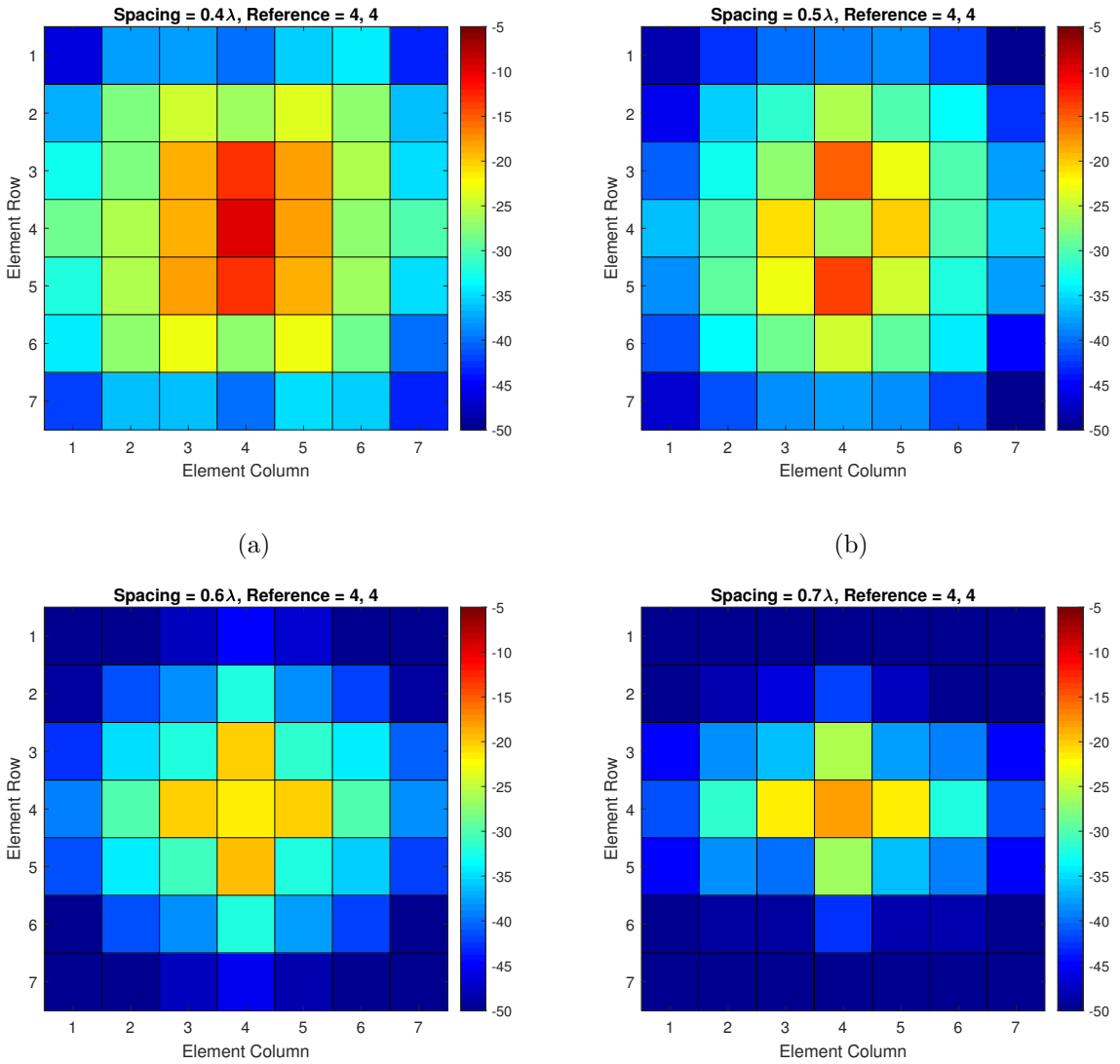

(a) (b)

(c) (d)

Figure 3.6: Coupling seen by the center element relative to all other elements. (a) 0.4λ element spacing. (b) 0.5λ element spacing. (c) 0.6λ element spacing. (d) 0.7λ element spacing.

It is shown in figure 3.6 that the highest levels of mutual impedance will be from neighboring elements, but not all elements will have a full ring of neighboring elements like the center element does. Corner and edge elements will not have the

same number of bordering elements which result in asymmetric mutual impedance effects along certain dimensions.

3.4.2 Element Position

Proximity to the edge of the array not only impacts diffraction fields seen in section 3.3, but mutual coupling will change to a degree as well. In the infinite array each element will experience the same amount of coupling regardless of position. However, in the finite array, element position will mean that elements closer to the edge will have fewer elements in close proximity and uneven amount of mutual impedance.

A dual-polarized 8x8 element microstrip patch array was designed and simulated with an infinite ground plane to eliminate edge effects and observe changes in mutual coupling. Similar to figure 3.4, radiation patterns have been plotted for a corner, edge, and center element in the array. Results seen in figure 3.7 show how the mutual coupling will change the radiation characteristics of element based on the position. Diffraction fields are not present, so most notably no ripples are introduced into co-polar radiation patterns and edge elements have fairly symmetric patterns. Cross-polarization levels in the E-plane for both the egde and corner elements are increased because inter-element is now asymmetric due to the element position.

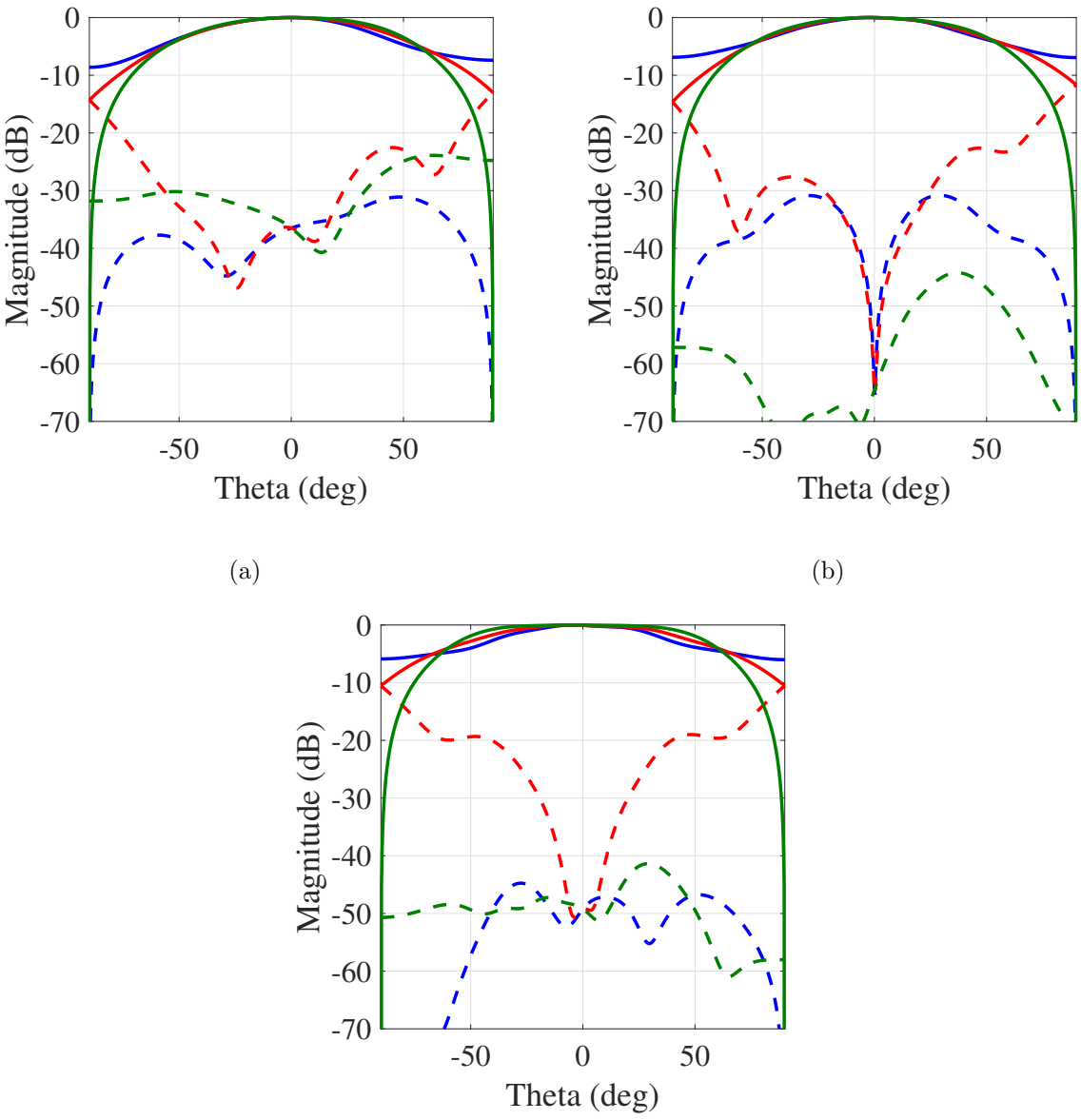

Figure 3.7: E-plane (blue), D-plane (red), and H-plane (green) co-polar (solid) and cross-polar (dashed) embedded element radiation patterns in an 8x8 element array located at (a) corner (b) edge (c) center.

Admittedly the impacts of mutual coupling on array embedded element patterns are minor compared to how diffraction fields impact radiation characteristics, however

results are consistent. When either mutual coupling or diffraction fields are asymmetric along a dimension performance radiation characteristics will be impacted.

3.5 Active Reflection Coefficient

The active or scanned reflection coefficient has proven to be a very useful tool in determining array scanning performance. For the infinite array, it can be easily obtained through simulation using floquet port analysis and simply varying theta and phi scan angles. The result will show reflections that the array will experience when scanning at various angles. For a finite array, the active reflection can be calculated for each element using a traditional scattering matrix. This means that scanning performance of a manufactured array can be calculated without the need to install phase shifters and measure the radiation pattern in a near-field or far-field system. In this section, the process of calculating the scanned reflection coefficient will be detailed for the case of a typical finite array. This process will then be repeated for a dual-polarized differential-fed 8x8 element array.

As discussed earlier in Chapter 3, there are a multitude of factors that are impacted by the finite size of the array. Mutual coupling, element geometry, array lattice, diffraction fields, and other variables will change resulting in changes in scanning performance related to array size. For these reasons, it is impossible to come to a single closed-form solution that will predict scanning range for every single array. However, it is very clear that the size of the array will change the active reflection coefficient in the array and therefore no longer agree with the unit cell. In this section

the array unit cell will be used to obtain the active reflection coefficient of the infinite array. Finite arrays of varying sizes will then be modeled and simulated to compare changes in the active reflection coefficient that result due to finite size.

The purpose of this array is to illustrate the changes in the active reflection coefficient that result because of the finite array size. As such, a rather simple single polarized probe-fed microstrip patch antenna will be used for the unit cell. The patch is then designed and tuned to resonate at 3 GHz. The **x** and **y** dimensions of the unit cell are chosen to be $\lambda/2$ so that half-lambda spacing is used for the infinite array. The unit cell is then simulated and scanned along the principle planes to obtain the active reflection coefficient for the infinite array.

The scanned reflection coefficient of the infinite array seen in figure 3.8 is to be expected. The array is well matched at broadside, but reflections increase as the scanning angle becomes more extreme. If wider scanning angles were desired, there are techniques that can be used to impedance match the antenna with the scan angle, but that is beyond the scope of this thesis. As scanning approaches $\theta = 90°$, the active reflection coefficient approaches unity because the ground plane is infinite and therefore it is impossible to scan any further.

The active reflection coefficient was then calculated for finite arrays of varying sizes using scattering parameters and the theory explained in Chapter 2. Results for 3x3, 5x5, 7x7, and 9x9 element arrays are shown in figure 3.9. When the array size is smaller, the array experiences less reflections at higher scan angles in part due to decreased ground plane size.

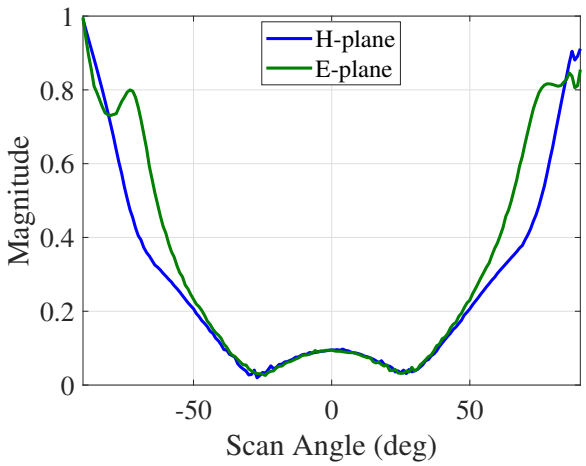

Figure 3.8: The active reflection coefficient of an infinite array of single-polarized microstrip patch antenna.

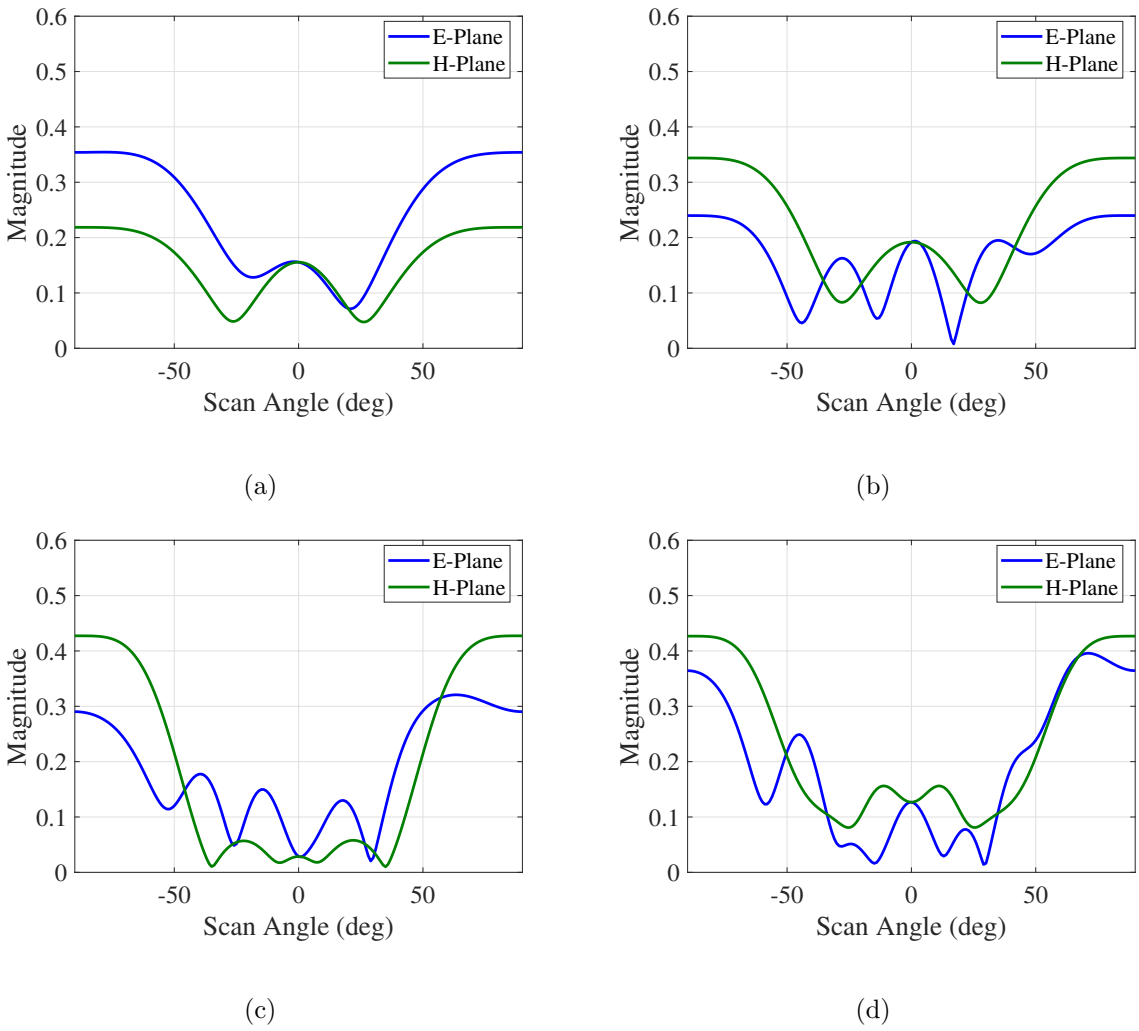

Figure 3.9: Calculated active reflection coefficient of the center element of a finite array of varying size (a) 3x3 array. (b) 5x5 array. (c) 7x7 array. (d) 9x9 array.

3.6 Scanning Performance

A fully assembled array system will typically be composed of smaller sub-arrays which are typically around the size of 8 by 8 elements in size. The goal of this section is to understand the impacts that this finite size will have on the scanning performance of the array. So far this chapter has been primarily focused on factors that impact the radiation characteristics. Diffraction fields resulting from the introduction of edge effects in the array will introduce ripples in co-polar radiation patterns as well as increases in cross-polar radiation levels. Mutual coupling will change the resonant frequency of an element as well as increase cross-pol radiation levels depending on the position. These factors will now be taken into consideration to show how finite size will impact the array.

In a large array, the full array pattern will approximately be the array factor multiplied by the isolated element pattern. Array elements are then given a progressive phase shift to accomplish beam-steering. In the finite array, the approximation using an isolated element will not be valid because diffraction fields and mutual coupling need to be accurately accounted for. When testing a single LRU in an anechoic chamber, the array will clearly be finite and performance will suffer, but this will not necessarily reflect performance that will be seen when the array is fully assembled. It is then necessary to create a model of the array that isn't as impacted by edge-effects that will not be seen in the full array. This can be done by using measured radiation patterns in the LRU to create an average embedded element for the array.

As previously discussed, an 8 by 8 LRU has been simulated and embedded element patterns have been obtained for the finite array. The array was also simulated using only a single element that was shifted into corresponding element positions to obtain isolated element patterns which show the impacts of edge effects on element radiation. Figures 3.10, 3.11, and 3.12 show the radiation patterns of each individual element inside the 64 element array with and without mutual coupling.

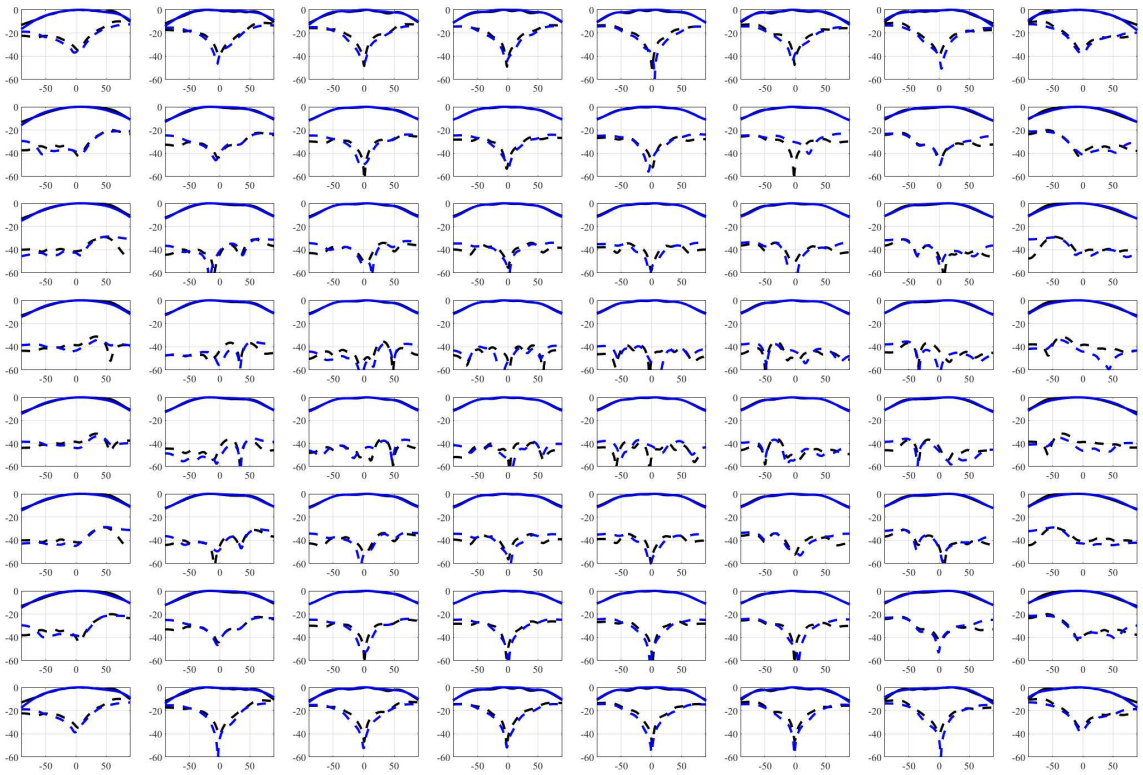

Figure 3.10: E-plane V-pol normalized radiation patterns for each element at 3 GHz when all others terminated in an 8x8 dual-polarized array (blue) compared to the radiation pattern of the isolated element (black) at the same position. Co-pol (solid) and cross-pol (dashed). In all plots in this figure, the y-axis represents magnitude of the radiation pattern of each element (dB) and the x-axis represents the radiation angle in the E-plane.

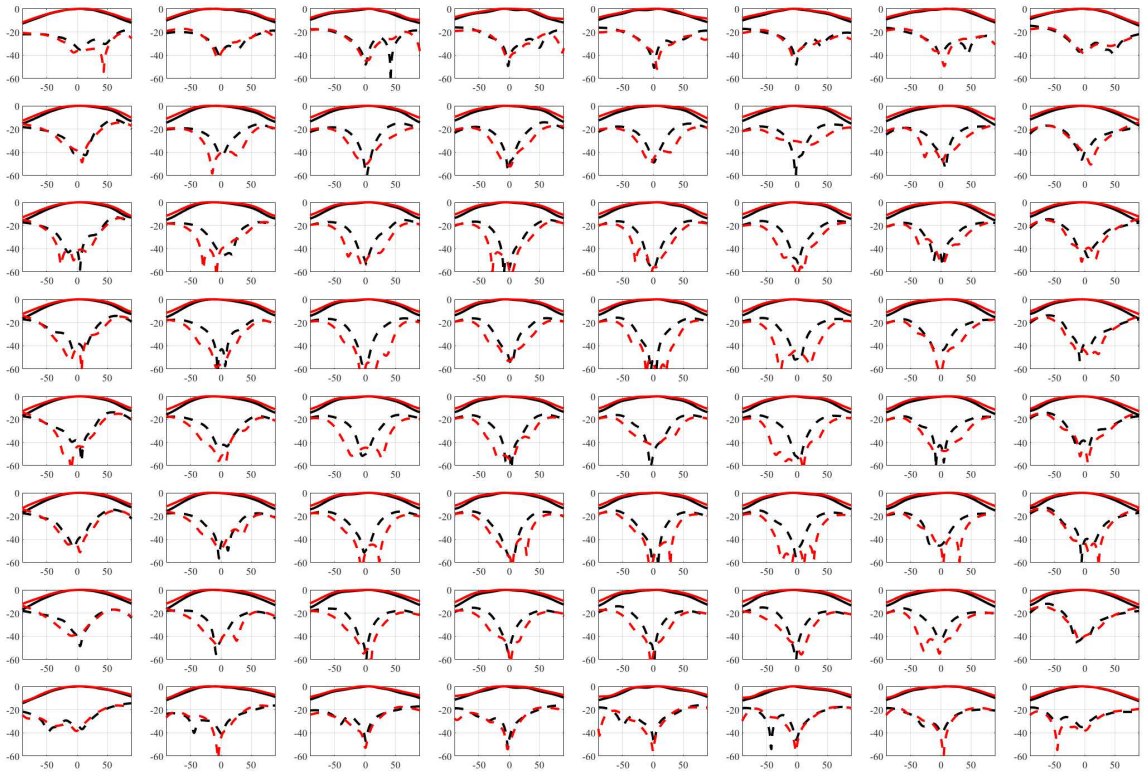

Figure 3.11: D-plane V-pol normalized radiation patterns for each element at 3 GHz when all others terminated in an 8x8 dual-polarized array (red) compared to the radiation pattern of the isolated element (black) at the same position. Co-pol (solid) and cross-pol (dashed). In all plots in this figure, the y-axis represents magnitude of the radiation pattern of each element (dB) and the x-axis represents the radiation angle in the D-plane.

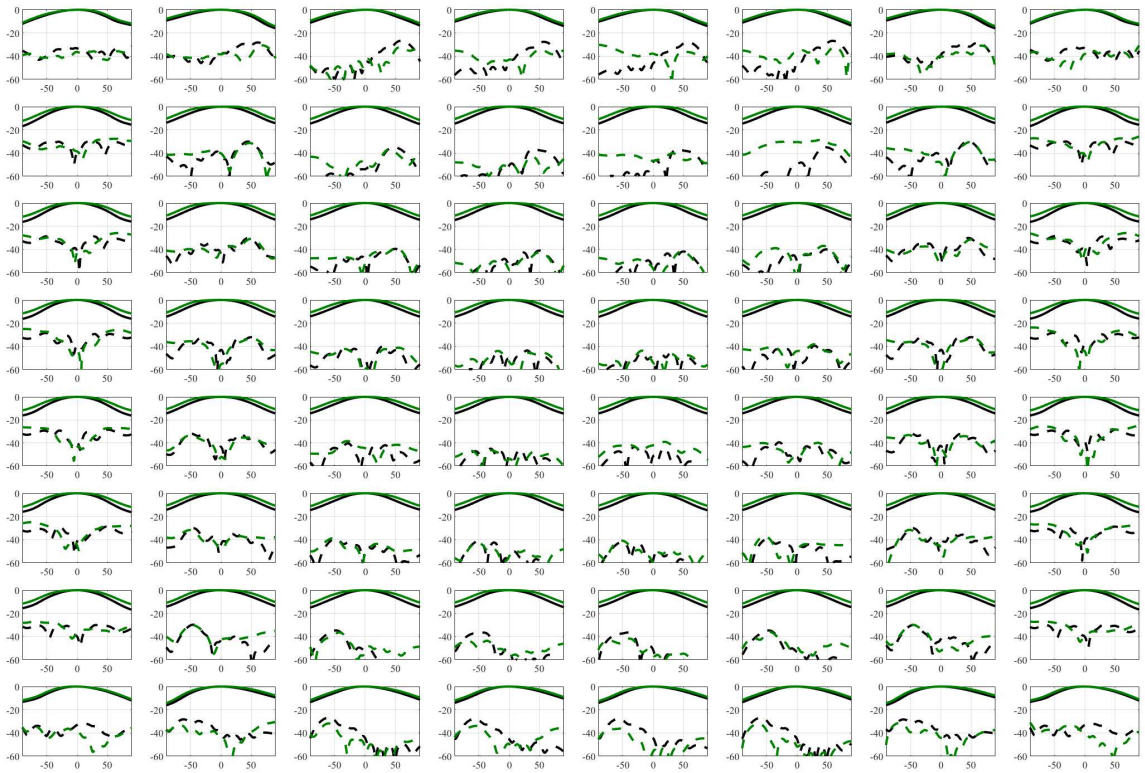

Figure 3.12: H-plane V-pol normalized radiation patterns for each element at 3 GHz when all others terminated in an 8x8 dual-polarized array (green) compared to the radiation pattern of the isolated element (black) at the same position. Co-pol (solid) and cross-pol (dashed). In all plots in this figure, the y-axis represents magnitude of the radiation pattern of each element (dB) and the x-axis represents the radiation angle in the H-plane.

Each element has its own unique radiation pattern which is ultimately impacted by both mutual impedance and edge effects within the array. To predict the scanning performance of the finite array, it is not possible to just use a single element within the array because it will not accurately account for the edge effects of the finite array. Instead, it is proposed that an average element pattern is obtained where each individual element pattern is phase shifted into the center position of the array and averaged together to create a single pattern using all elements within the array.

Pattern averaging will be discussed in more detail in Chapter 4, but it will be used here briefly.

Array radiation patterns for a large array can be estimated by multiplying the element pattern of the isolated pattern by the array factor. For a finite array, a single center element can be used as well, but an average element pattern multiplied by the array factor will give a more accurate prediction of the full pattern as demonstrated in Chapter 4. As illustrated in Figure 3.13, the embedded element pattern of each element in an 8x8 S-band array is overlapped with the average of all elements for each cut (E-, D-, H-plane) at 3 GHz. In the E-plane, the co-polar embedded element patterns are very similar presenting a variability in gain of about ± 2 dB at ± 45 degrees. However, the cross-polar embedded element patterns are significantly different for each element in the array and in each cut. From element to element, cross-pol can change around ± 10 dB. This is mainly attributed to diffraction fields due to symmetry of each element with respect to the edges of the ground plane.

In the D-plane (Figure 3.13b), co-polar patterns are even less sensitive than in the E-plane with a variability of ± 1 dB at ± 45. However, little change is seen in the cross polarization levels and variability is about ± 5 dB. This is not because there are no diffraction fields, but the cross-polarization levels are very high in comparison to the diffraction fields.

In the H-plane (Figure 3.13c), the cross-pol levels are very similar to the E-plane. This is because a microstrip patch antenna with a differential feed is being used. Embedded element co-polar patterns have a variability of ± 1 dB at ± 45. However, the cross-polarization changes significantly depending on element position. In this

case, cross-pol variance is about ±15 dB. The reason for the high variability is because the cross-pol is aligned to the fields of the patch in the E-plane.

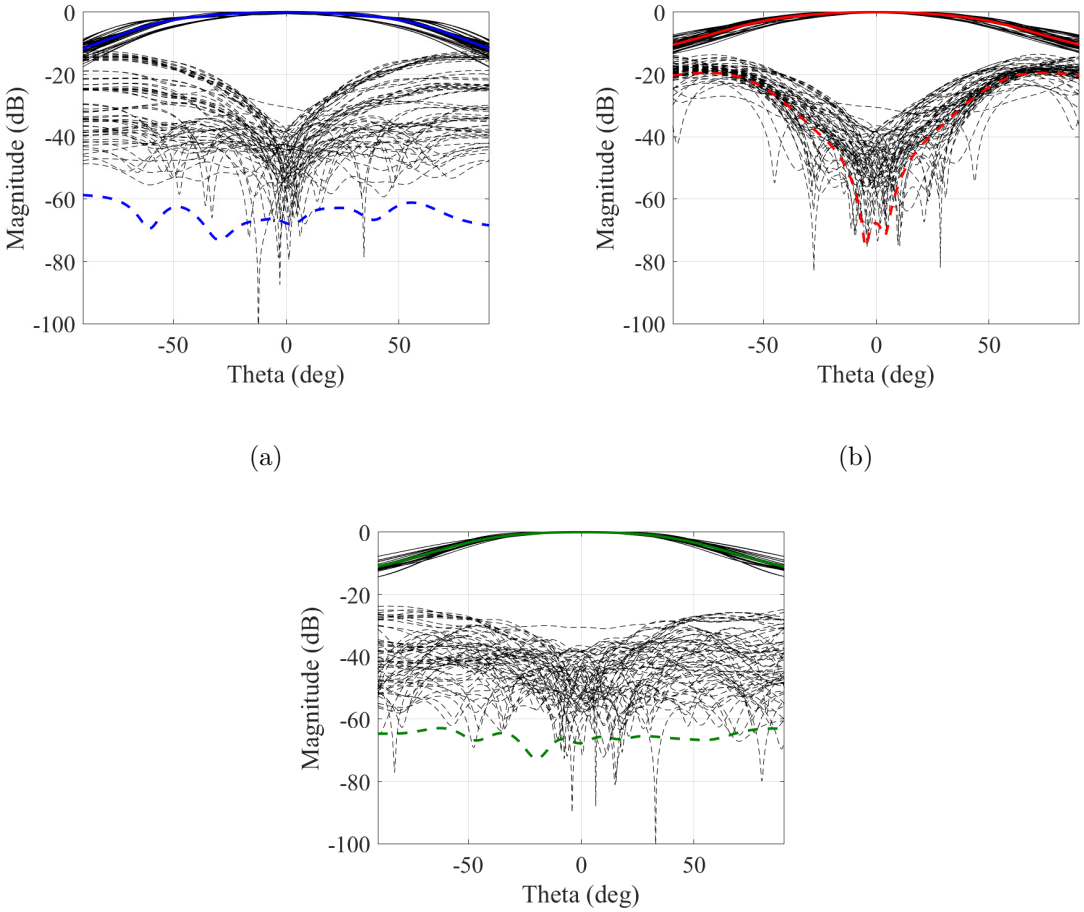

Figure 3.13: Overlapped embedded element patterns (black) for 8x8 array at 3 GHz with its average radiation pattern (colored) for a finite vertically polarized array. (a) E-plane, (b) D-plane, (c) H-plane. Co-pol (solid), cross-pol (dashed).

3.7 Summary

Finite array antennas will ultimately suffer from edge effects and differences in element radiation characteristics depending on the position of the element in the array.

Diffraction fields will result in more significant changes seen in both co- and cross-pol radiation patterns, but mutual coupling will do this as well. Both of these factors are greatly impacted by the symmetry in the array. For instance, a center element will experience roughly the same amount of diffraction fields and mutual coupling along each plane. When this symmetry is lost, uneven mutual impedance and diffraction fields will result in increased cross-polarization levels. To accurately represent the finite array diffraction fields should not be ignored by representing the full array with an isolated element pattern multiplied by the array factor. Instead, all individual embedded element patterns can be averaged together to result in a single average element pattern. In the next chapter, pattern averaging will be explored more in depth and used to predict the performance of the full array.

Chapter 4

Array Scanning Prediction

4.1 Introduction

The radiation characteristics of array line-replaceable units (LRU) are normally tested outside of the full array and therefore diffraction fields on a single sub array will be more prevalent than what will be seen in the full array. To accurately represent the performance of the full array, an average embedded element can be obtained from the array adding element patterns together along with a phase shift to electrically shift the element to the center of the array. Ultimately it is desired to average element patterns to obtain an average element pattern that will resemble the average pattern seen in the full array.

4.2 Average Element Pattern

The resulting average element pattern will depend on the number of patterns added together. The overall goal of the average embedded element patterns is to determine a appropriate number of elements that should be averaged in order to obtain a pattern resembling the embedded element pattern seen in the full array pattern when all LRUs are assembled. The average element pattern will first be used along rows and columns in the array to show when cross-polarization cancellation occurs. The antenna used

for this experiment will be an 8x8 element dual-polarized microstrip patch array which will be vertically polarized. Figure 4.1 shows the layout of the array.

1	2	3	4	5	6	7	8
9	10	11	12	13	14	15	16
17	18	19	20	21	22	23	24
25	26	27	28	29	30	31	32
33	34	35	36	37	38	39	40
41	42	43	44	45	46	47	48
49	50	51	52	53	54	55	56
57	58	59	60	61	62	63	64

Figure 4.1: Dual-polarized 8x8 element array.

First, the rows of the array will be averaged. If a single row is averaged together, no cross-polarization cancellation will occur. This is because the array is polarized along the rows, so there is no destructive interference occurring in cross-polarization patterns. In other words, for cross-pol cancellation to occur, elements need to be added along the plane orthogonal to the plane of polarization. In this case, the array is polarized along the rows of the array so an array column needs to be average for cross-polarization cancellation to occur. For example, in figure 4.2a the first row is averaged and the average cross-polarization pattern does not decrease. The same result is seen when the last row of the array (row eight) is averaged in figure 4.2b. As stated, for this polarization elements in the same column need to be averaged so that element cross-polarization patterns will destructively interfere and result in a lower average cross-polarization pattern. It would then stand to reason that averaging both

the other rows of the array (rows one and eight) would then result in a decrease of the average cross-polarization levels as seen in figure 4.2c.

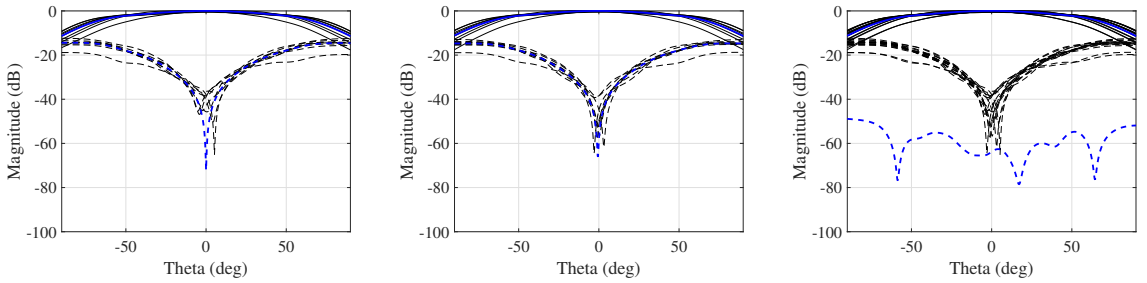

(a) (b) (c)

Figure 4.2: The embedded radiation pattern of each element in an 8x8-element vertically polarized microstrip patch array antenna and the average radiation pattern at 3 GHz in the E-plane using (a) row one, (b) row eight, and (c) rows one and eight. Co-pol (solid), cross-pol (dashed), embedded radiation patterns (black), and average radiation pattern (blue).

Averaging the array along plane of cross-polarization (array columns) will mean that cross-pol cancellation will occur, but the average co-polarization patterns will not accurately represent the performance of the full array because there will be no addition along the plane of co-polarization. The average co-pol pattern along a column will be impacted by uneven diffraction fields from edge effects resulting in an asymmetrical average co-pol radiation pattern. This is demonstrated in average E-plane radiation patterns of column one in figure 4.3a and the average E-plane patterns of column eight in figure 4.3b. When both columns one and eight are averaged as in figure 4.3c. The edge effects will cancel and result in a symmetric co-pol radiation pattern.

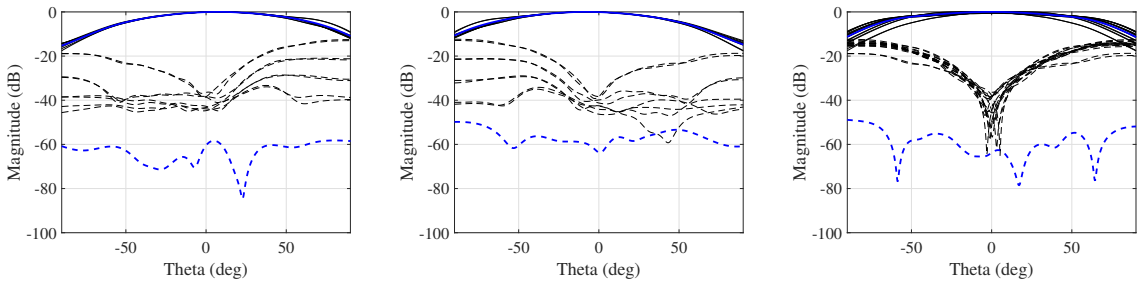

(a) (b) (c)

Figure 4.3: The embedded radiation pattern of each element in an 8x8-element vertically polarized microstrip patch array antenna and the average radiation pattern at 3 GHz in the E-plane using (a) column one, (b) column eight, and (c) columns one and eight. Co-pol (solid), cross-pol (dashed), embedded radiation patterns (black), and average radiation pattern (blue).

Averaging the H-plane of the array elements will yield similar results to the E-plane. However, since the H-plane is orthogonal to the E-plane, the planes in which co- and cross-polarization occur will now be switched. This will mean that cross-polarization cancellation will occur in the H-plane when a row is averaged. Figures 4.4a and 4.4b show averaging along rows one and eight, respectively. It can be noted that the co-polar radiation patterns are asymmetric edge effects. When both rows one and eight are averaged together in figure 4.4c, edge effects will be symmetric resulting in a symmetric co-polar pattern in the H-plane.

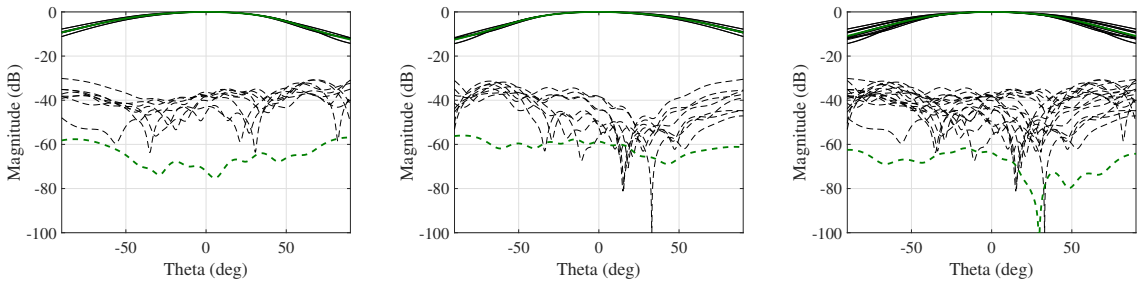

(a) (b) (c)

Figure 4.4: The embedded radiation pattern of each element in an 8x8-element vertically polarized microstrip patch array antenna and the average radiation pattern at 3 GHz in the H-plane using (a) row one, (b) row eight, and (c) rows one and eight. Co-pol (solid), cross-pol (dashed), embedded radiation patterns (black), and average radiation pattern (green).

It will then be seen that averaging along the columns of the array in the H-plane will result in pattern addition along the plane of co-polarization in the H-plane. Cross-pol cancellation will not occur as seen in the E-plane. The result will mean that edge effects will be even in the co-pol patterns but not in cross-polarization patterns. Averaging either column one or column eight in figures 4.5a and 4.5b, respectively, will result in uneven cross-polarization cancellation. However, when both columns are averaged together as in figure 4.5c, cancellation will occur and the averaged cross-polarization pattern will be decreased.

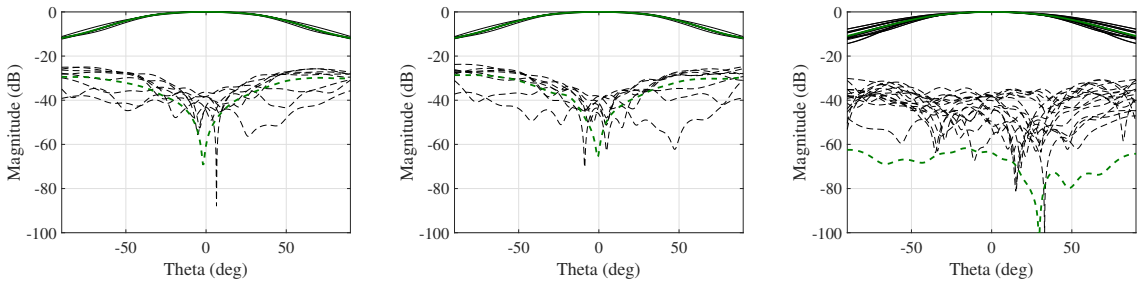

(a) (b) (c)

Figure 4.5: The embedded radiation pattern of each element in an 8x8-element vertically polarized microstrip patch array antenna and the average radiation pattern at 3 GHz in the H-plane using (a) column one, (b) column eight, and (c) columns one and eight. Co-pol (solid), cross-pol (dashed), embedded radiation patterns (black), and average radiation pattern (green).

The same averaging done for both the E- and H-planes will not result in cross-polarization cancellation in the diagonal plane. In both the E- and H-planes, cross-pol cancellation occurs when patterns are averaged along the dimension of the array orthogonal to the corresponding. However, if the same process of averaging is done along the rows and columns with the diagonal plane, this does not happen.

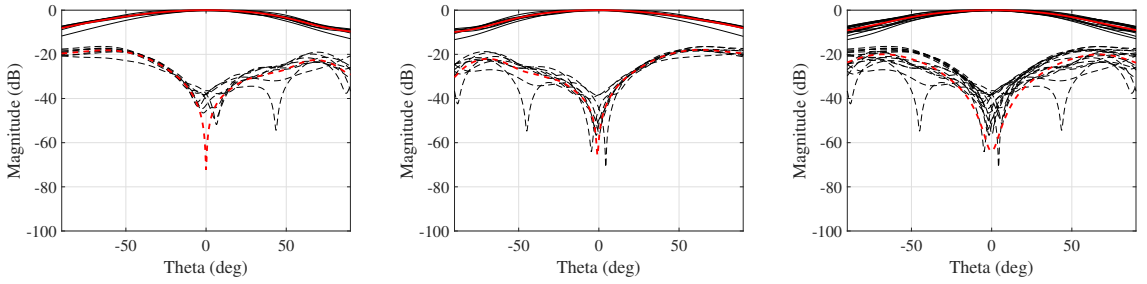

(a) (b) (c)

Figure 4.6: The embedded radiation pattern of each element in an 8x8-element vertically polarized microstrip patch array antenna and the average radiation pattern at 3 GHz in the D-plane using (a) row one (b) row eight, and (c) rows one and eight. Co-pol (solid), cross-pol (dashed), embedded radiation patterns (black), and average radiation pattern (red).

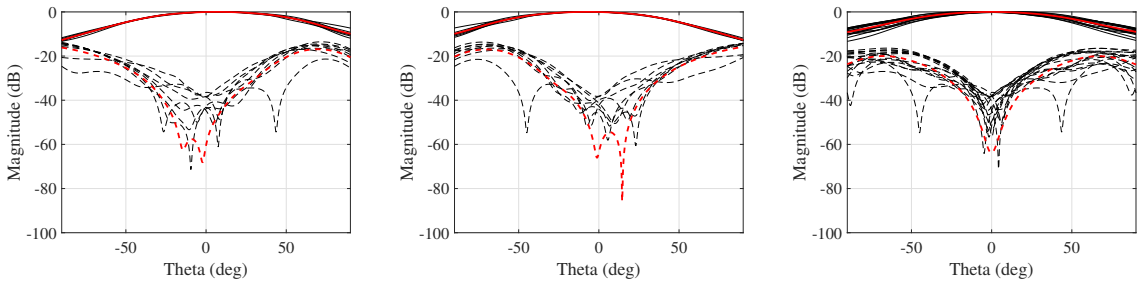

(a) (b) (c)

Figure 4.7: The embedded radiation pattern of each element in an 8x8-element vertically polarized microstrip patch array antenna and the average radiation pattern at 3 GHz in the D-plane using (a) column one, (b) column eight, and (c) columns one and eight. Co-pol (solid), cross-pol (dashed), embedded radiation patterns (black), and average radiation pattern (red).

4.3 Full Array Scanning

It has been shown that to obtain an accurate average element pattern, there needs to be symmetry in the elements chosen to be averaged so that both the co- and cross-pol patterns average in the principle planes to reduce the impacts of diffraction fields from edge effects. In this section, various sub-arrays will be averaged within a single LRU will be averaged to obtain a single average element pattern to accurately represent both the co- and cross-polarization patterns that will be seen when all the LRUs and assembled to create the full array.

Using the traditional isolated element pattern multiplied by the array factor of the antenna will not accurately reflect the cross-pol seen in the full array. When the isolated is placed on a finite ground plane as in figure 4.8, cross-polarization levels will be drastically increased due to edge effects, but in reality when the LRUs are assembled these edge effects will be decreased. Alternatively, if the radiation patterns

of an isolated element on an infinite ground plane are used to create the full array patterns, no edge effects will be included in the resulting patterns. It is necessary to average the array elements to allow for diffraction fields to cancel due to the symmetry of the array.

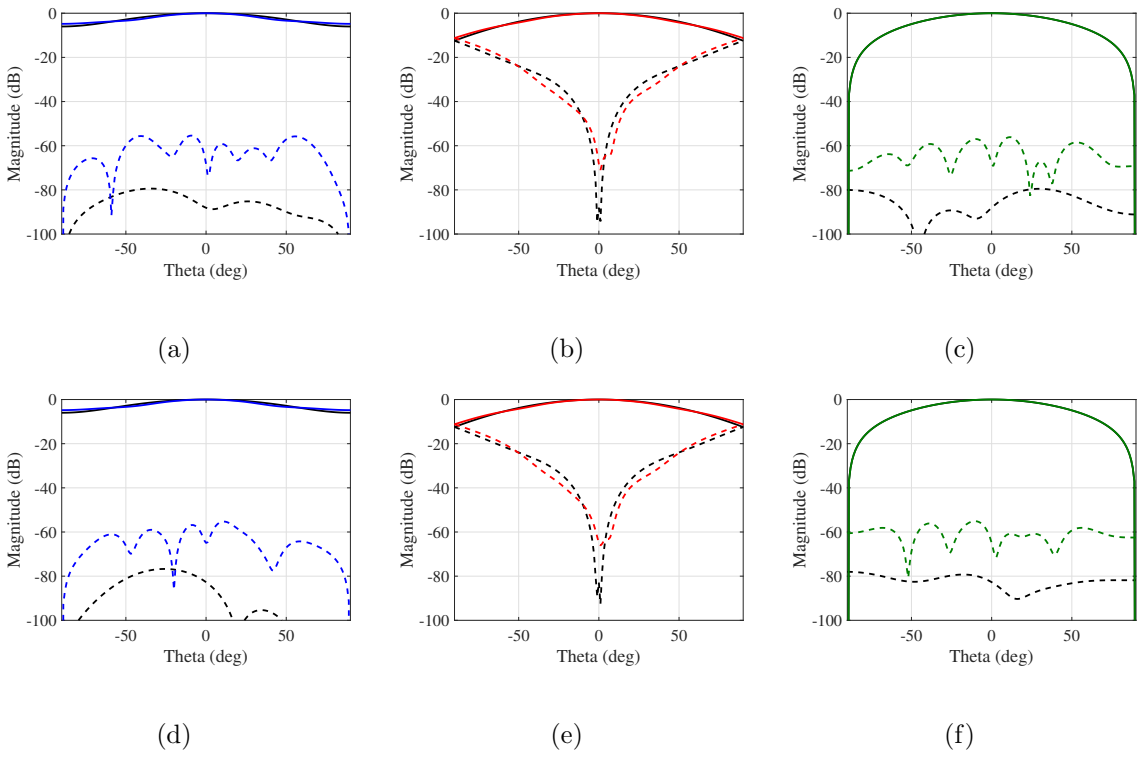

Figure 4.8: Co-pol (solid) and cross-pol (dashed) radiation patterns for an isolated element on an infinite ground plane (black) and a finite ground plane (colored) for the E-plane (blue), D-plane (Red), and H-plane (Green) which the microstrip patch is vertically polarized (a-c) and horizontally polarized (d-f).

Averaging the entire finite array will lead to an excessive presence of diffraction fields in the resulting patterns, thus inaccurately representing the full array performance. Alternatively, when the outer elements of the array are terminated and the rest are averaged it is possible to better predict the average element pattern for the full array. When the full array is assembled it will contain 64 individual 8x8 element

subarrays for a total of 4096 dual-polarized elements. Unfortunately, due to computational limitations, it was not possible to obtain an average element pattern for the full array, so the 8x8 element array was simulated with an infinite ground plane and the elements were averaged together. This case will be used as an approximation for the average patterns of the full array. Subsections of the finite array will then be used to attempt to predict this pattern.

The resulting average array patterns are seen in figure 4.9. Again the goal is to use the finite array patterns to replicate the average array patterns of the 8x8 array with an infinite ground plane. The sub-arrays within the LRU were chosen such that the array is symmetric along the principle planes to allow for the cancellation of diffraction fields introduced due to the finite size of the array. As such, it was chosen to terminate the outer ring of elements first to result in a 6x6 finite array with a ring of dummy elements. This process was then repeated to obtain a 4x4 array with two rings of dummy elements and finally a 2x2 element array with three rings of dummy elements. The resulting sub-arrays were then averaged and compared to the reference 8x8 element array radiation patterns with an infinite ground plane.

Figure 4.9 indicates that terminating the outer two rings of elements (4x4 sub-array) will result in a pattern that most accurately represents the full 64x64 element array. It is common to terminate all array elements except for the very center elements to predict full array performance, but this is not enough elements to allow for cancellation of diffraction fields. Cross-polarization levels were highest when this method was chosen.

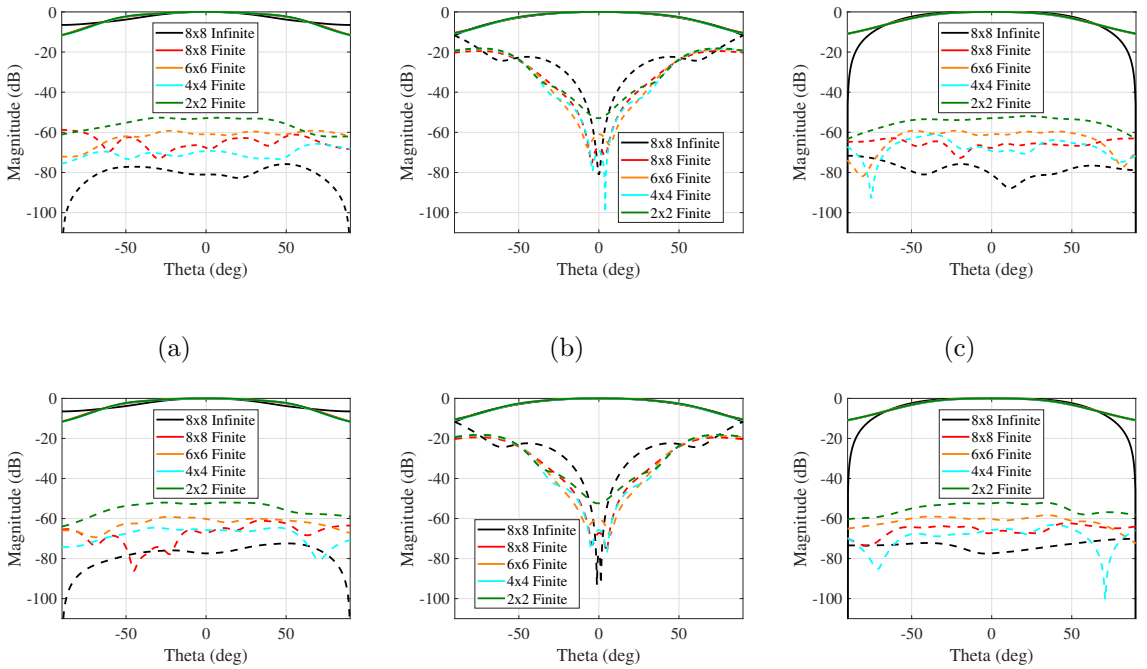

Figure 4.9: Co-pol (solid) and cross-pol (dashed) average radiation patterns for microstrip patch antenna LRU sub-arrays for the E-plane (blue), D-plane (Red), and H-plane (Green) which the element is vertically polarized (a-c) and horizontally polarized (d-f).

With an accurate predication of what the full array average element pattern will be, the array factor can then used to reproduce the patterns expected in the full 64x64 element array as shown in figure 4.10. The array factor can be phase shifted and multiplied by this average element pattern to approximate full array scanning performance. While this method can be used to predict co-polar radiation patterns, the main benefit of this method is that it provides a more accurate method to predict the cross-pol radiation patterns of the full array.

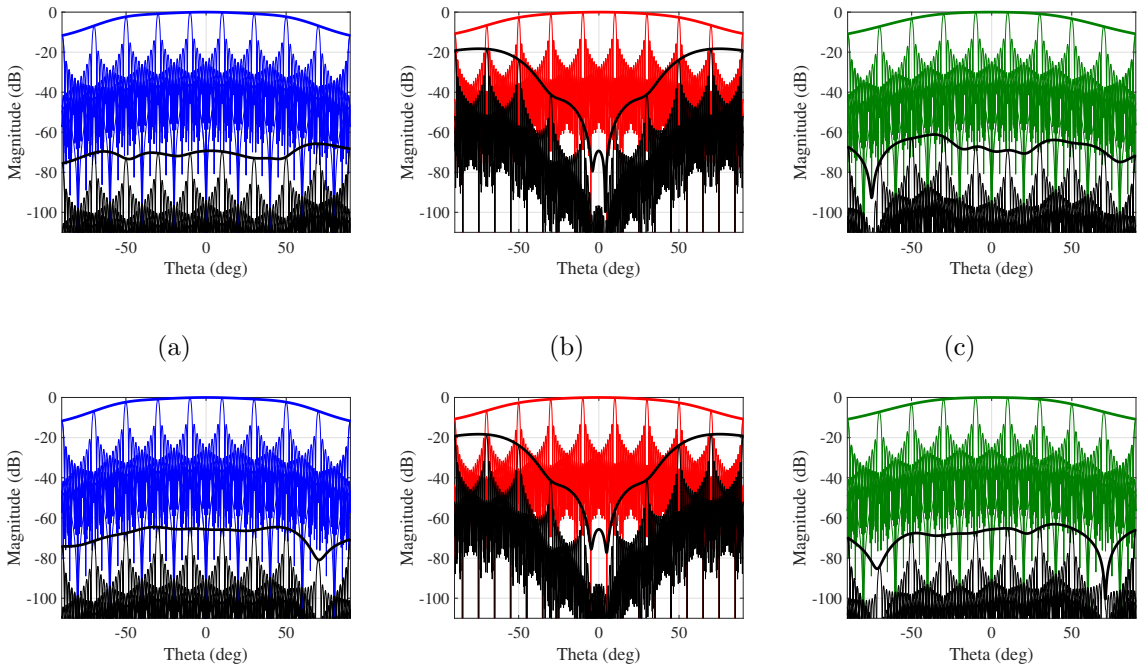

Figure 4.10: Co-pol (colored) and cross-pol (black) scanned radiation patterns for a 64 element microstrip patch array for the E-plane (blue), D-plane (Red), and H-plane (Green) which the element is vertically polarized (a-c) and horizontally polarized (d-f).

4.4 Summary

The use of the average element pattern allows for cancellation of diffraction fields in the principle planes due to pattern addition. For this cancellation to occur an element needs to be averaged with a symmetric element in the plane of interest. For co-pol patterns to be symmetric, an element should be averaged with the pattern of the element along the same principle plane, but on the opposite side of the array. For cross-pol pattern to be symmetric, an element should be averaged with opposite element along the plane orthogonal to the desired principle plane. To obtain a good

average pattern there should be both proper symmetry and as many elements as possible.

To represent the scanning performance of the full array, the use of the average element pattern was employed. Different sub-arrays within the LRU were averaged to obtain a pattern that most accurately represents the average element patterns of the full array. The elements averaged in the LRU were chosen to allow for diffraction field cancellation, and the outer two rings of elements were terminated to decrease the edge effects seen in the finite array. Finally, the average element pattern was then scanned to predict the full array scanning performance.

Chapter 5

Conclusions and Future Work

5.1 Conclusion

This thesis project focuses on analyzing how the finite size of a measured array LRU will impact the scanning performance of the subarray. When radiation patterns are obtained for the LRU in an anechoic chamber, the array will not be in the same infinite array environment in which it is was designed or intended to operate, so they will not necessarily indicate the performance of fully assembled array.

This project has demonstrated that diffraction fields from edges will impact the radiation characteristics of a finite microstrip patch array antenna. Diffraction fields were shown to be sensitive to both element position and ground plane size. For instance, when a patch is located at the center of a ground plane it will experience symmetric diffraction fields. However, when the patch is offset from the center of the array, asymmetric edge effects will change ripple size in co-polar radiation patterns and cross-polarization levels will be increased. In short, diffraction fields mean that each element will placed in a finite environment.

As such, a method of pattern averaging has been proposed as a more accurate way to predict the full array co- and cross-polarization patterns of the full array by terminating edge elements within the LRU and then electrically shifting the embedded

element patterns to the center of the array so that they can be averaged to create a single average element pattern which is then multiplied by the array factor to approximate the full array patterns.

5.2 Future Work

The results presented in this thesis were obtained using simulations of phased array antennas. In particular, a dual-polarized differential-fed 8x8 element array was simulated to predict scanning performance when placed into a larger 64x64 element array. Averaging a smaller subarray of the 8x8 element array resulted in cancellation of edge effects and a decrease in the predicted cross-polarization levels. It was not possible to obtain a physical antenna to test this analysis on, but it is possible that due to errors in both the manufacturing and measurement processes that the measured phase of each embedded element pattern will not be as precise meaning that measured patterns will not be as symmetric and simulated results and less cancellation diffraction fields from edge effects may occur.

Bibliography

[1] D. S. Zrnic and R. J. Doviak, "System requirements for phased array weather radar," *NOAA/NSSL Rep*, 2005.

[2] J. I. Echeveste, M. A. González de Aza, and J. Zapata, "Array pattern synthesis of real antennas using the infinite-array approach and linear programming," *IEEE Transactions on Antennas and Propagation*, vol. 63, no. 12, pp. 5417–5424, 2015.

[3] J. L. Salazar, E. Loew, P. Tsai, J. Vivekanandan, W. C. Lee, and V. Chandrasekar, "Design trade-offs for airborne phased array radar for atmospheric research," in *2013 IEEE International Symposium on Phased Array Systems and Technology*, pp. 371–378, 2013.

[4] H. A. Wheeler, "The radiation resistance of an antenna in an infinite array or waveguide," *Proceedings of the IRE*, vol. 36, pp. 478–487, April 1948.

[5] H. Wheeler, "Simple relations derived from a phased array made of an infinite current sheet," in *1964 Antennas and Propagation Society International Symposium*, vol. 2, pp. 157–160, Sep. 1964.

[6] P. Carter, "Mutual impedance effects in large beam scanning arrays," *IRE Transactions on Antennas and Propagation*, vol. 8, pp. 276–285, May 1960.

[7] J. Allen, "Gain and impedance variation in scanned dipole arrays," *IRE Transactions on Antennas and Propagation*, vol. 10, pp. 566–572, Sep. 1962.

[8] L. Kurtz, R. Elliott, S. Wehn, and W. Flock, "Mutual-coupling effects in scanning dipole arrays," *IRE Transactions on Antennas and Propagation*, vol. 9, pp. 433–443, Sep. 1961.

[9] P. Hannan, P. Meier, and M. Balfour, "Simulation of phased array antenna impedance in waveguide," *IEEE Transactions on Antennas and Propagation*, vol. 11, pp. 715–716, November 1963.

[10] M. Balfour, "Active impedance of a phased-array antenna element simulated by a single element in waveguide," *IEEE Transactions on Antennas and Propagation*, vol. 15, pp. 313–314, March 1967.

[11] S. Edelberg and A. Oliner, "Mutual coupling effects in large antenna arrays: Part 1–slot arrays," *IRE Transactions on Antennas and Propagation*, vol. 8, pp. 286–297, May 1960.

[12] L. Stark, "Radiation impedance of a dipole in an infinite planar phased array," *Radio Science*, vol. 1, pp. 361–377, March 1966.

[13] G. Farrell and D. Kuhn, "Mutual coupling effects in infinite planar arrays of rectangular waveguide horns," in *1966 Antennas and Propagation Society International Symposium*, vol. 4, pp. 392–397, Dec 1966.

[14] D. Pozar and D. Schaubert, "Scan blindness in infinite phased arrays of printed dipoles," *IEEE Transactions on Antennas and Propagation*, vol. 32, pp. 602–610, June 1984.

[15] W. Gregorwich, A. Hessel, and G. Knittel, "A waveguide simulator study of a blindness effect in a phased array (waveguide simulator study of blindness/resonance or surface wave/effect in phased array antennas)," *Microwave Journal*, vol. 14, pp. 37–41, 1971.

[16] A. K. Bhattacharyya, *Phased Array Antennas: Floquet Analysis, Synthesis, BFNs and Active Array Systems*, vol. 179. John Wiley & Sons, 2006.

[17] D. M. Pozar, "The active element pattern," *IEEE Transactions on Antennas and Propagation*, vol. 42, pp. 1176–1178, Aug 1994.

[18] B. Diamond, "Small arrays - their analysis and their use for the design of array elements," *Phased Array Antennas*, pp. 127–131, 1972.

[19] W. Wasylkiwskyj, "Mutual coupling effects in semi-infinite arrays," in *1972 Antennas and Propagation Society International Symposium*, vol. 10, pp. 169–172, Dec 1972.

[20] A. Ishimaru, R. Coe, G. Miller, and W. Geren, "Finite periodic structure approach to large scanning array problems," *IEEE Transactions on Antennas and Propagation*, vol. 33, no. 11, pp. 1213–1220, 1985.

[21] R. C. Hansen, "Evaluation of the large array method," *IEE Proceedings H - Microwaves, Antennas and Propagation*, vol. 137, no. 2, pp. 94–98, 1990.

[22] A. K. Bhattacharyya, "Floquet modal based approach for mutual coupling between elements in array environment," in *IEEE Antennas and Propagation Society International Symposium. 1996 Digest*, vol. 3, pp. 1908–1911 vol.3, 1996.

[23] D. Pozar, "Analysis of finite phased arrays of printed dipoles," *IEEE Transactions on Antennas and Propagation*, vol. 33, no. 10, pp. 1045–1053, 1985.

[24] B. Avser and V. B. Erturk, "A new method for the prognosis of scan blindness angle in finite phased arrays of printed dipoles," in *Proceedings of the 5th European Conference on Antennas and Propagation (EUCAP)*, pp. 1014–1017, 2011.

[25] V. B. Erturk, O. Bakir, R. G. Rojas, and B. Guner, "Scan blindness phenomenon in conformal finite phased arrays of printed dipoles," *IEEE Transactions on Antennas and Propagation*, vol. 54, no. 6, pp. 1699–1708, 2006.

[26] B. Sanadgol, O. Litschke, and K. Solbach, "Method to predict scan blindness in printed planar phased arrays," in *2009 3rd European Conference on Antennas and Propagation*, pp. 3105–3108, 2009.

[27] R. J. Mailloux, *Phased Array Antenna Handbook*. Artech House, 2017.

[28] C. A. Balanis, *Antenna Theory: Analysis and Design*. John Wiley & Sons, 2016.

[29] Y. Mushiake, "A report on Japanese development of antennas: from the Yagi-Uda antenna to self-complementary antennas," *IEEE Antennas and Propagation Magazine*, vol. 46, no. 4, pp. 47–60, 2004.

[30] E. O. Hammerstad, "Equations for microstrip circuit design," in *1975 5th European Microwave Conference*, pp. 268–272, 1975.

[31] W. L. Stutzman and G. A. Thiele, *Antenna Theory and Design*. John Wiley & Sons, 2012.

[32] R. C. Johnson and H. Jasik, *Antenna Engineering Handbook*. McGraw-Hill, 1984.

[33] R. C. Hansen, *Phased Array Antennas*, vol. 213. John Wiley & Sons, 2009.

[34] D. M. Pozar, *Microwave Engineering 3e*. Wiley, 2006.

[35] A. Fenn, G. Thiele, and B. Munk, "Moment method analysis of finite planar phased antenna arrays," in *1979 Antennas and Propagation Society International Symposium*, vol. 17, pp. 633–636, June 1979.

[36] S. Edelberg and A. Oliner, "Mutual coupling effects in large antenna arrays II: Compensation effects," *IRE Transactions on Antennas and Propagation*, vol. 8, pp. 360–367, July 1960.

[37] M. Balfour, "Phased array simulators in waveguide for a triangular arrangement of elements," *IEEE Transactions on Antennas and Propagation*, vol. 13, pp. 475–476, May 1965.

[38] V. de la Rubia, J. Zapata, and M. A. Gonzalez, "Finite element analysis of periodic structures without constrained meshes," *IEEE Transactions on Antennas and Propagation*, vol. 56, pp. 3020–3028, Sep. 2008.

[39] G. H. Knittel, A. Hessel, and A. A. Oliner, "Element pattern nulls in phased arrays and their relation to guided waves," *Proceedings of the IEEE*, vol. 56, pp. 1822–1836, Nov 1968.

[40] G. V. Borgiotti, "Modal analysis of periodic planar phased arrays of apertures," *Proceedings of the IEEE*, vol. 56, pp. 1881–1892, Nov 1968.

[41] V. W. H. Chang, "Infinite phased dipole array," *Proceedings of the IEEE*, vol. 56, pp. 1892–1900, Nov 1968.

[42] K. M. Pasala and E. M. Friel, "Mutual coupling effects and their reduction in wideband direction of arrival estimation," *IEEE Transactions on Aerospace and Electronic Systems*, vol. 30, pp. 1116–1122, Oct 1994.